This is the accepted version of Stutenbecker, L., Costa, A., Bakker, M., Anghileri, D., Molnar, P., Lane, S.N. and Schlunegger, F., 2019. Disentangling human impact from natural controls of sediment dynamics in an Alpine catchment. Earth Surface Processes and Landforms, 44, 2885-2902
A typeset copy is available at : https://rdcu.be/bVZNI

Disentangling human impact from natural controls of sediment dynamics in an Alpine catchment

Laura Stutenbecker[1,2*], Anna Costa[3,4], Maarten Bakker[5,6], Daniela Anghileri[3,7], Peter Molnar[3], Stuart N. Lane[5], Fritz Schlunegger[1]

[1] Institute of Geological Sciences, University of Bern, 3012 Bern, Switzerland

[2] Institute of Applied Geosciences, Technical University Darmstadt, 64287 Darmstadt, Germany

[3] Institute of Environmental Engineering, ETH Zürich, 8093 Zürich, Switzerland

[4] Alaska Climate Research Center, University of Alaska Fairbanks, 99775 Fairbanks, Alaska (USA)

[5] Institute of Earth Surface Dynamics, University of Lausanne, 1015 Lausanne, Switzerland

[6] Irstea, ETNA, University Grenoble Alpes, Grenoble, France

[7] Department of Geography and Environment, University of Southampton, SO17 1BJ Southampton, United Kingdom

* Corresponding author. Email: stutenbecker@geo.tu-darmstadt.de

Abstract

Human activities have increasingly strong impacts on the sediment dynamics of watersheds, directly, for example through water abstraction and sediment extraction, but also indirectly through climate change. This study aims at disentangling these impacts on natural sediment fluxes for the Borgne river, located in the Alps of South-

West Switzerland, using two approaches: First, an assessment of contemporary sediment sources and their relative contribution to the sediment delivered to the catchment outlet is undertaken by geochemical fingerprinting and a mixing model. Second, a spatially distributed conceptual model of suspended sediment production and transfer is used to quantify the contribution of different portions of the catchment to the total sediment yield. The model describes the influence of hydroclimatic variables (rainfall, snowmelt, and ice melt), water diversions and reservoir trapping on the sediment yield accounting for the erodibility of the different land covers present in the catchment. The analysis of different scenarios based on this conceptual model aids the interpretation of the fingerprinting results and the identification of the most important factors controlling sediment fluxes. Although the conceptual model overestimates the contribution of the downstream source area and underestimates the contribution of the upstream source area, the results allow us to qualitatively assess the impacts of different drivers influencing the sediment yield at the catchment scale. The results suggest: (1) high sediment yield from the uppermost part of the catchment due to sediment delivery by glacial ice melt; (2) delayed sediment transfer from areas impacted by water abstraction; and (3) reduced sediment contribution from areas upstream of a major hydropower reservoir that intercepts and traps sediment. Although process (1) and processes (2) and (3) serve to counter one another, our study emphasizes that the relative impacts of Anthropocene climate change and human impacts on sediment delivery may be disentangled through multi-proxy approaches.

Introduction

Tectonically active mountain belts can be considered the most important suppliers of water and clastic sediment on our planet mainly because of their large topographic gradients and associated high erosion rates, and active mass wasting processes (Hovius et al., 1997; Montgomery & Brandon, 2002; Tucker & Slingerland, 1996; Willett, 1999). Rivers are the most important transport and distribution systems that connect these sediment sources with their sinks. The quantities of water and sediment provided by fluvial networks can considerably affect landscape evolution (e.g. by triggering mass wasting processes; Korup, 2009), biogeochemical cycles (e.g. by transporting nutrients or carbon; Stallard, 1998), and biodiversity (e.g. by providing natural habitats to flora and fauna; Wohl, 2006).

In Central Europe, the Alpine orogen is one of the most important sediment factories due to its high relief and denudation rates. Its water and sediment feeds major European fluvial networks such as the Rhine, Rhône, Po, and Danube rivers. However, like many mountainous regions, the Alps are increasingly affected by climate change, which result in accelerated glacial retreat (Costa et al., 2018a; Fischer et al., 2015; Scherrer & Appenzeller, 2006; Serquet et al., 2011) as well as increased rates of hillslope erosional activity (Micheletti et al., 2015). In parallel, mountainous environments are directly impacted by humans through land-use, for example through deforestation and reforestation, and river management (e.g., Anselmetti et al., 2007; Comiti, 2012; Niedrist et al., 2009; Weber et al., 2007; Wohl, 2006). Yet, we know very little about the net effects of these processes on sediment delivery downstream, on their temporal and spatial variability, and of the feedback mechanisms that exist between them. This is particularly the case for the Swiss Rhône valley, where water fluxes have been heavily managed and regulated particularly through the construction of hydropower dams and flow intake systems (Bakker et al., 2018; Gabbud & Lane, 2016). Despite the strong anthropogenic perturbation, only a very few studies have considered the possible effects of these water management practices in recent years on downstream sediment delivery (Loizeau & Dominik, 2000, Lane et al., 2019).

Here, we focus on the catchment of the Borgne, a tributary of the Rhône river, where dynamic landscape responses to water abstraction have already been documented (Bakker et al., 2018; Gabbud & Lane, 2016; Lambiel et al., 2016; Lane et al., 2014, 2017; Micheletti et al., 2015; Micheletti & Lane, 2016; Reynard et al., 2012). The main goals of this study are (1) to trace the current fine-grained sediment flux in the catchment through a geochemical fingerprinting approach and (2) to assess the sensitivity of sediment production and transfer processes to anthropogenic disturbances. To achieve this aim, we compare results of sediment fingerprinting with simulations of a spatially distributed conceptual model for suspended sediment load based on hydroclimatic variables. The spatially distributed conceptual model is partially based on previous work (Costa et al., 2018b), where the suspended sediment production from each cell in the modelled catchment domain is simulated by considering controlling factors, including hydroclimatic forcing (rainfall, snowmelt, ice melt), surface erodibility, anthropogenic water management, and sediment trapping. This modelling framework is then applied for a number of scenarios, and the role of the different controlling factors is assessed by comparing the simulated sediment composition at the outlet with the measured one.

Setting

Physiography

The Borgne catchment is the third-largest tributary of the Swiss Rhône river, which drains one of the largest intramontane catchments located in the Pennine Alps of southwestern Switzerland (Fig. 1). The Borgne catchment has a total size of 385 km^2 and can be divided into two main valleys, the eastern Val d'Hérens and the western Val d'Hérémence (Fig. 1). The altitude in the catchment ranges between 492 and 4346 m above sea level (a.s.l.), with a mean elevation of 2390 m a.s.l. According to the CORINE land cover classification, more than half of the land cover is classified as open space with little or no vegetation, followed by shrub and/or herbaceous vegetation association (ca. 22%), forest (ca. 17%), pastures (ca. 5%) and inland waters (ca. 1%) (Table 1). About 11% of the total catchment area is glaciated today and most glaciers are located at higher altitudes in the uppermost one third of the catchment (Table 1).

Climate

The Borgne catchment is characterized by a typical Alpine intramontane climate. We analyse precipitation and temperature patterns in the catchment based on spatially distributed datasets provided by the Swiss Federal Office for the Environment, at ~ 2×2 km^2 resolution grid for the period 1975-2017 (Frei et al., 2006; Frei, 2014; Schwarb, 2000). The mean annual precipitation computed over the observation period 1961-2017 is 1097 mm/y and shows an orographically-driven spatial distribution with relatively drier conditions at the lower altitudes (minimum of 688 mm/y) and wetter conditions (maximum of 2008 mm/y) at higher altitudes. The mean annual daily temperature is -0.7 °C, and is likewise characterized by a strong spatial variability between the lower and higher altitudes, 7°C and -6°C, respectively. In the late 1980s and early 1990s, the study area has experienced a substantial increase in mean annual air temperature (Bakker et al., 2018; Costa et al., 2018a). Rapid glacial retreat following temperature warming has been reported for many Alpine glaciers during the last decades (Fischer et al., 2014; 2015), including the ones located in the study area such as the Glacier de Tsijiore Nouve, the Glacier de Ferpècle and the Haut Glacier d'Arolla (Gabbud et al., 2016; GLAMOS, 2017).

Water and sediment abstraction

The Borgne catchment is one of the tributaries of the Swiss Rhône river most affected by human impacts. The construction of a major hydropower dam, the Grande Dixence was completed in Val d'Hérémence in 1961. The associated lake, the Lac de Dix (Fig. 1), has a water storage capacity of 400 billion m^3 (Lane et al., 2014). Water is supplied not only from the ~45 km^2 large catchment of the lake itself, but also from the neighbouring valleys through a network of 100 km of transfer tunnels and pumping stations (Bakker et al., 2018; Anghileri et al., 2018 a; b; Lane et al., 2014; Margot et al. 1992). The water intakes are equipped with sediment traps for both fine- and coarse-grained material, from which sediment is flushed down the river at frequencies up to several times per day (Bakker et al., 2018; Lane et al., 2017). In addition, sediment is mined along the Borgne river channel at least at four locations (Lane et al., 2014). Data from local authorities indicate that this mostly concerns coarse-grained sediment (gravel), but these data are not publicly available.

Geology

The Central Alps formed during the collision of the European continental margin in the North and the Adriatic microplate in the South, thereby closing the so-called Penninic domain in between (Schmid et al., 2004). The Penninic nappes consisted of a northern marine trough, the Valais Ocean and a southern oceanic basin, the Piedmont-Liguria Ocean, which were separated from each other by the Briançonnais microcontinent. The bedrock of the Borgne catchment is made up of three tectonic units (Fig. 2, Table 1). The uppermost 31% of the catchment area is underlain by gneisses and minor meta-gabbroic and meta-sedimentary rocks of the Austroalpine (Adriatic) Dent Blanche complex. The middle reaches (ca. 32%) are made of calcschists ("Bündnerschiefer") and meta-basaltic rocks of the Piedmont-Liguria Ocean. The lowermost 37% of the catchment contain the meta-sedimentary cover (quartzites, schists, marbles and conglomerates) as well as gneisses of the Briançonnais microcontinent (Federal Office of Topography Swisstopo, 2011).

Thick Quaternary glacial tills deposited predominantly during the Last Glacial Maximum (LGM) are widespread, especially in the lowermost parts of the catchment (Fig. 2). Geomorphological and sedimentological field observations suggest that most of these tills are moraine deposits sourced by tributary valley glaciers (Lambiel et al., 2016).

Methods

We identify the provenance of suspended sediment through a sub-catchment fingerprinting approach. The relative contribution of the various sub-catchments to the total fine sediment load is then estimated through mixing modelling. In parallel, we estimate the hydroclimatic controls on the transfer of material through modelling. Based on Costa et al. (2018b), our conceptual model assumes that there are three main hydroclimatic factors driving the suspended sediment regime in Alpine environments: (1) total daily erosive rainfall, defined as liquid precipitation over snow-free surfaces, (2) total daily snowmelt, and (3) total daily ice melt. Erosive rainfall enables hillslope erosion, channel erosion through increased streamflow, and is responsible for triggering mass wasting events (e.g. landslides and debris flows), which release large amounts of sediment. Overland flow produced by snowmelt contributes to hillslope erosion as well as to channel erosion through increased streamflow. Ice melt flows carry high concentrations of glacially-derived sediment from sub-glacial channels and proglacial areas. Costa et al. (2018b) demonstrated how all three hydroclimatic factors contribute to suspended sediment dynamics, but exhibit different contributions in the entire Swiss Rhône catchment. They showed that while total daily catchment-averaged ice melt, rich in fine sediment, generates the largest contribution to the total annual suspended sediment yield at the outlet of the catchment, total daily catchment-averaged erosive rainfall is responsible for the peaks in mean daily suspended sediment concentration and consequently determines its variability.

Spatial datasets

We extract topographic and geologic variables (watershed outlines, stream network, glacial cover, lithologies, land cover) using standard topographic and hydrologic tools within ArcGIS© version 10.1. The 2-m-resolution digital elevation model swissALTI^{3D} (Federal Office of Topography Swisstopo, 2014), the 1:500,000 geological map (Federal Office of Topography Swisstopo, 2011) and the CORINE land cover map (Steinmeier, 2013) are used as base maps. Precipitation, minimum, maximum and mean daily air temperature data are available on a ~ 2×2 km^2 resolution grid for Switzerland for the period 1975-2017 (Frei et al., 2006; Frei, 2014; Schwarb, 2000).

<u>Sediment source fingerprinting</u>

Sediment was sampled at the outlets of several sub-catchments, where we assume that the samples represent a natural mixture of all upstream lithologies (tributary sampling approach, see for example Garzanti et al., 2012; von Blanckenburg, 2005). Within each of the lithological units defined above, two to three sub-catchments were chosen based on the lithological architecture of the Borgne catchment (Fig 2). These are the Borgne d'Arolla and Borgne de Ferpècle for the gneiss end-member, the Satarma, Bornetta and Gavil streams for the calcschist/meta-basalt end-member and the Grand Torrent, Manna and Torrent de Faran streams for the meta-sedimentary end-member. Composite sediment samples were collected from the river bed close to the outlet of the tributary rivers on one occasion in June 2016, assuming that the fingerprint of the relatively small sub-catchments (7-40 km^2) would be relatively stable throughout the year. To obtain relative contributions of the source end-members to the catchment-wide sediment budget samples were taken at the Borgne river mouth close to the village of Bramois (Figs. 1, 2). In contrast to the small sub-catchments, the chemical composition of sediment in the main river is more likely to be variable through time (e.g., due to anthropogenic activities, but also natural sediment storage, sorting effects and provenance changes). In order to monitor possible compositional changes through time, five samples were taken throughout the year 2016 (February, June, July, August, October) at the same location.

The Quaternary glacial deposits may contribute largely to the catchment output, because they are only weakly consolidated and thus easily erodible. Field observations suggest that the tills were sourced by tributary valley glaciers and formed without significant reworking or sediment entrainment/ mixing from higher units. However, in order to test this hypothesis and to exclude any affects related to reworking, which could impact the fingerprinting results, a glacial till sample from a large, fresh and unvegetated outcrop was also taken and analysed (Fig. 2).

The sediment samples were wet-sieved into three grain size classes: <40 μm, 40-400 μm and >400 μm. No comprehensive grain size analysis was undertaken prior to geochemical analysis, but the weights of the three fractions were recorded. The 40-400 μm grain size fraction was milled using a planetary ball mill. Bulk geochemistry is determined for the <40 μm and 40-400 μm fractions by inductively coupled plasma mass spectrometry (ICP-MS) using lithium borate fusion at the Acme labs in Vancouver, Canada. The analytical package includes the major element oxides SiO_2, Al_2O_3, CaO, Fe_2O_3, MgO, Na_2O, K_2O, TiO_2, P_2O_5, MnO, Cr_2O_3, as well as the trace elements Ba, Ni, Sr, Zr, Y, Nb and Sc. All results are corrected for the loss of ignition (LOI). See supplementary material 1 for details on the standards used by the laboratory and the detection limits.

Principle Component Analysis (PCA) is used to visualize the data variance and to produce compositional biplots (Aitchison, 1983; Aitchison & Greenacre, 2002). Log-ratio transformed biplots are created using the software CoDaPack (Comas & Thió-Henestrosa, 2011). Following standard statistical methods, the data are analysed in order to identify the key characteristics discriminating the three defined sources (Collins et al., 1996; Collins & Walling, 2002; Smith & Blake, 2014). First, elements used as input variables in a mixing model should behave conservatively between the sediment source and the catchment outlet. Elements that get enriched or depleted during transport or deposition, for example through hydrologic sorting or chemical dissolution, do not fulfil this requirement. Thus, elements that show higher or lower concentrations in the sample taken at the Borgne outlet compared to the source end-member compositional range are removed from the fingerprinting dataset. Second, elements should provide statistically significant discrimination between the source end-members. To test which elements are suitable to distinguish the three lithological units defined here, the non-parametric Kruskal-Wallis H-test is used, with a threshold p-value of 0.05. Finally, stepwise Discriminant Function Analysis (DFA) identifies a combination of elements that provides the greatest discrimination between the sources based on the minimisation of Wilks' lambda (Collins & Walling, 2002; Smith & Blake, 2014).

In order to estimate the relative contributions of the three end-member sources to the sediment sampled at the Borgne outlet, a mixing model developed by Laceby & Olley (2015) is used and solved with the Optquest algorithm in Oracle's software CrystalBall. The algorithm tests different end-member contributions P_s and finds the best solution by minimizing the Mixing Model Difference (MMD) between simulated and observed composition:

$$MMD = \sum_{i=1}^{n}(C_i - (\sum_{s=1}^{m} P_s \cdot S_{si})) \div C_i \qquad \text{(Eq. 1)},$$

where n is the number of fingerprinting elements chosen as input parameters, i is a fingerprinting element, C_i is the concentration of the element i in the Borgne outlet sample, m is the number of sources s in the catchment (in this case s = 3), P_s the relative contribution (%) of each source s, and S_{si} the concentration of element i in the source s.

The uncertainties of source contributions, based on the variability in element concentrations, are estimated using a Monte Carlo sampling routine with 10,000 iterations. Normal distributions are calculated for each element and each of the three sources. The mean value of the 10,000 iterations thus represents the mean proportional contribution of each source, with the standard deviation representing the uncertainty. The goodness of fit (GOF) of the mixing modelling results is quantified based on the difference of the observed and modelled catchment outlet composition (Laceby & Olley, 2015).

Conceptual modelling of sediment sources dynamics

Based on Costa et al. (2018b), we develop a spatially distributed framework for suspended sediment production and transfer to analyse the spatial and temporal variability of sediment dynamics. We consider the three main hydroclimatic forcing mechanisms that drive the suspended sediment regime in these environments: (1) total daily erosive rainfall (ER), defined as liquid precipitation over snow-free surfaces, (2) total daily snowmelt (SM), and (3) total daily ice melt (IM). As these three drivers represent the typical main forces acting in mountainous regions (see the discussion in Costa et al., 2018b), the model is widely applicable to alpine regions in general, although this work focuses particularly on the Borgne catchment. Since suspended sediment-related data are available only at the outlet of the Swiss Rhône catchment, first we calibrate the model on the entire Swiss Rhône catchment, and, in a second step, we apply the optimal parameter set to the Borgne catchment.

We test the pair-wise correlation between the hydroclimatic predictors at the cell scale. Average values of correlation coefficients over the available observation period (1975-2017) are equal to -0.04 between ER and SM, -0.1 between SM and IM, and 0.3 between ER and IM, indicating low inter-correlation amongst the hydroclimatic factors. We assume that sediment fluxes generated by these three variables contribute to suspended sediment yield in a complementary way, both in terms of timing and magnitude, because of the variety of sediment sources involved (e.g. hillslopes, channels, glaciers) and the diversity of the erosional and transport processes (e.g. soil erosion by raindrop impacts, soil detachment by snowmelt−driven overland flow). Although sediment erosion models are usually based on rainfall intensity at the sub-daily scale (e.g. Francipane et al., 2012; Morgan & Duzant, 2008; Wischmeier & Smith, 1978), we adopt a daily time scale due to data availability and the coarse temporal resolution of sediment sampling.. This is supported by the results of Costa et al. (2018b) which using an iterative input variable selection algorithm (Galelli & Castelletti, 2013; Denaro et al., 2017) to show that total daily catchment-averaged ER explains 75% of the variability of suspended sediment concentration at the Rhône river outlet, including total daily catchment-averaged IM and SM raises the explained variance of suspended sediment concentration up to 90%.

Suspended Sediment Production

We conceptualize suspended sediment load, $SSL_{i,t}$, produced in each cell *i* of the catchment per time step *t (*being the time resolution equal to *1 day)* as the sum of the contribution of the three hydroclimatic forcing expressed in the form of a rating curve (Eq. 2).

$$\mathrm{SSL_{i,t}} = A_i \cdot k_i \cdot \left[\mathrm{a_1} \cdot \mathrm{ER_{i,t}^{b_1+1}} + \mathrm{a_2} \cdot \mathrm{SM_{i,t}^{b_2+1}} + \mathrm{a_3} \cdot \mathrm{IM_{i,t}^{b_3+1}}\right] \cdot 10^7 \quad \text{(Eq. 2)}$$

Soil erodibility in each cell *i* is accounted for by the parameter k_i. Individual contributions of sediment load (e.g. $\mathrm{a_1} \cdot \mathrm{ER_{i,t}^{b_1+1}}$) are expressed in dag day^{-1} m^{-2}, A_i represents the cell surface in m^2, $SSL_{i,t}$ is expressed in ton day^{-1} and 10^7 is a unit conversion factor.

Suspended sediment transfer

Suspended sediment fluxes are linearly convoluted to the outlet of the catchment (Eq. 3) and integrated to contribute to the total suspended sediment load.

$$\mathrm{SSL_t^{outlet}} = \sum_{\mathrm{i=1}}^{\mathrm{nc}} (1-\beta_i) \cdot \mathrm{SSL_{i,t-\tau_i}} \quad \text{(Eq. 3).}$$

where $\mathrm{SSL_t^{outlet}}$ [ton day^{-1}] is the total suspended sediment load reaching the outlet of the catchment at time *t*, $\mathrm{SSL_{I,t-\tau_I}}$ is the sediment load generated at cell *i* at time $t-\tau_i$ computed as in Eq. 2, *nc* is the total number of cells in the catchment, τ_i [day] is the travel time of sediment at cell *i*, i.e. the time it takes for sediment produced at cell *i* to reach the outlet of the catchment. Coefficient β_i represents the degree of sediment dis-connectivity between cell *i* and the outlet. It expresses the fraction of the sediment produced at cell *i* that does not reach the outlet of the catchment, either because it is diverted to reservoirs and (semi-)permanently trapped. The latter case refers mainly to sediment that cannot be mobilized and transported due to the reduction in transport capacity associated with water abstraction schemes. Therefore, the coefficient 1-β_i expresses the fraction of the sediment actually contributing to the suspended sediment load at the outlet on a sub-annual time-scale. The travel time τ_i is a function of the distance of the cell *i* to the outlet, l_i [m], and the velocity of the sediment flux, v_i [m s^{-1}]. The velocity of each sediment flux produced at cell i, SSL_i, is based solely on cell i and it is assumed constant and equal to an average velocity from the source to the sink.$\tau_i = \frac{\mathrm{l_i}}{v_i}$

(Eq. 4).

Modelling of hydroclimatic variables

Total daily ER, SM and IM distributed over the entire Swiss Rhône catchment are estimated on the basis of gridded datasets of total daily precipitation and mean, maximum and minimum daily air temperature (Frei et al., 2006; Frei, 2014; Schwarb, 2000). Ice, snow accumulation and melting are modelled with a degree–day approach (e.g. Hock, 2003). Precipitation is divided into rainfall and snow based on a temperature threshold and rainfall is classified as erosive only on snow–free cells. Likewise, ice melt occurs only on glacier cells that are snow–free. The temperature thresholds for snow/rain division and for snow and ice melting are set equal to 1 °C and 0 °C respectively, based on previous studies in the catchment (e.g. Costa et al., 2018a; Fatichi et al., 2015). The parameters of the degree-day model are calibrated and validated on the basis of satellite–derived snow cover maps (MODIS) for the period 2000-2008 and observations of discharge measured at different locations within the Borgne catchment during the period 1975-2015. For more details on the hydroclimatic modelling as well as the calibration and validation procedure, see Costa et al. (2018a).

Reference scenario and parameter calibration

The catchment is divided into a regular grid of 500 m by 500 m cells (i.e. A_i = 500^2 m^2). For the current situation, which we refer to as "reference scenario", we consider that soil erodibility, k_i, is a function of land cover (Eq. 5). Starting from the CORINE land cover map (Steinmeier, 2013), we group land cover categories of the Swiss Rhône catchment into three main classes of level of erodibility, in order to maintain a low number of model parameters and preserve the spatial variability in soil erodibility: (1) forest, wetlands, waterbodies and artificial surfaces such as non-agricultural vegetated areas, urban fabric, industrial, commercial and transport units (the categories are named as in the CORINE datasets) are grouped into a low erodibility class, covering almost 24% of the entire catchment; (2) pastures, arable land, heterogeneous agricultural areas, permanent crops, and mine, dump and construction sites are grouped into a medium erodibility class, covering roughly 31% of the surface; and (3) open space with little or no vegetation, which covers almost 45% of the catchment, is considered part of a high erodibility class. Each erodibility class is characterized by a unique value of erodibility, k_l, with $l = 1, 2, 3$, where k_1, k_2 and k_3 are model parameters, representing respectively low, medium and high soil erodibility. To account for the high denudation rates that characterize glaciers (Hallet et al., 1996), we assume a multiplicative factor, α_g, for cells that are partially or fully covered by glaciers.

$$k_i = \begin{cases} k_l \cdot \alpha_g & if\ cell\ is\ a\ glaciated\ cell \\ k_l & otherwise \end{cases} \quad \text{(Eq. 5)}$$

A detailed schematic of hydropower infrastructures operating in the Swiss Rhône catchment is available from Fatichi et al. (2015). Based on this information, we divide the catchment into cells that are regulated by hydropower and those that are not. We further divide cells regulated by hydropower into two categories: cells that are flowing directly into reservoirs, and cells that lie upstream of water intakes. We assume that all suspended sediment produced in cells that are not impacted by hydropower reaches the catchment outlet ($\beta_i = 0$ in Eq. 3), while suspended sediment generated in cells that flow directly into reservoirs is entirely trapped and does not reach the outlet ($\beta_i = 1$ in Eq. 3). This is appropriate as Lac de Dix is not currently flushed. Based on measurements of suspended sediment concentrations (Bakker, 2018), it is expected that only a fraction of the sediment originated at cells upstream of intakes reaches the outlet. First, only the washload is, at least partially, diverted to the reservoirs together with the water flow. Second, the reduced transport capacity downstream of water intakes due to water abstraction may reduce the amount of sediment delivered to downstream reaches and the rate at which this occurs (Bakker et al. 2018). For cells *i* draining into water intakes, we identify the value of the coefficient β_i to be equal to 0.5, based on the following analysis, and supported by results from Bakker (2018). We calibrate the model parameters, using the procedure described below, with multiple values of the parameter β_i and we choose the value producing the highest model performance. We discuss the limitation of these assumptions at the end of the paper.

Sediment transfer rates are expected to differ among regulated and unregulated cells. In particular, sediment that is intercepted by gravel and sand traps is only transferred downstream during flushing events. Therefore, sediment transfer rates are expected to be much slower than under natural flow conditions. To allow sediment flux velocities to be spatially distributed, we assume that the velocity of the sediment fluxes originated in cells that are not regulated is constant in time and within the unregulated domain, and is equal to the parameter v_{nat} [m s^{-1}]. For cells upstream of hydropower infrastructures, we assume that the fraction of suspended sediment load that actually gets to the outlet is travelling at a different velocity, which we model to be constant in time and within the regulated area, and equal to the parameter v_{div} [m s^{-1}]. We are aware that effects of water abstraction on sediment transport will also impact downstream reaches. However, in this analysis we assume that stream flow and suspended sediment transport capacity increases rapidly with distance downstream from intakes due to the contribution of overland flow from hillslopes, unregulated tributaries and groundwater. As such sources are not glaciated, we assume that these have lower sediment loads than the glacial melt flows which are abstracted.

We calibrate the twelve parameters of the model that are the soil erodibility parameters, k_1, k_2, and k_3, the α_g parameter, accounting for high denudation rates in glaciated areas, the two parameters representing sediment flux velocities v_{nat} and v_{div}, and the remaining six parameters of the hydroclimatic multivariate rating curve (Eq. 2), a_i and b_i with i = 1, 2, 3, by minimizing the root mean squared error between mean daily values of suspended sediment load at the outlet of the Swiss Rhône catchment, simulated in the “reference scenario” and derived from observations over the period from 01 May 2013 until 30 April 2017. Target values of mean daily suspended sediment load at the outlet of the Swiss Rhône catchment are estimated by multiplying measured mean daily discharge and mean daily suspended sediment concentration derived, on the basis of a calibrated power law relation, from observations of turbidity collected at the outlet of the catchment (Costa et al., 2018b).

We adopted a leave-one-year-out cross-validation approach by splitting the available dataset into a split calibration-validation test to avoid overfitting given the limited observation datasets. We thus conducted four calibrations and validations over periods of three and one years, respectively (see Table A1 in the supplementary material 2). To calibrate the model parameters, we use an optimization approach based on a genetic algorithm. We repeat the optimization procedure 50 times, starting from randomly generated initial values to reduce the possibility of finding sub–optimal parameter configurations. For the remaining analysis of this work, we adopt the parameter values of the tests performing best in validation in terms of root mean squared error. We will refer to this parameter set as the optimal parameter set in the following.

Testing scenarios

In a second step, we use the optimal parameter set obtained in calibration for the "reference scenario" on the entire Swiss Rhône, to simulate mean daily suspended sediment load values at the outlet of the Borgne catchment, during the period 1975-2017, for different scenarios (Table 5). We estimate the sediment composition at the outlet by separating the sediment originated in the three different lithological units (Fig. 2) and we compare model simulations with results of the sediment fingerprinting analysis. To assess the impact of the different controlling factors, we test multiple scenarios (Table 5), starting from a simple configuration and progressively adding factors such as land cover, glaciers, hydropower reservoirs and water diversions until reaching the "reference scenario", representing the current state. The comparison between the different scenarios allows us to qualitatively evaluate the impact of the controlling factors on the sediment composition at the outlet of the Borgne catchment.

In the first scenario, we model a uniform land cover, characterized by low erodibility (i.e. $k_i = \mathrm{k}_1 \; \forall \, i$) for the entire Borgne catchment. We do not consider the larger sediment supply in glaciated areas α_g (i.e. α_g = 1) or the effect of hydropower, thus neither reservoirs nor water intakes are operating (i.e. $\beta_i = 0 \; \forall \, i$, $\mathrm{v}_{\mathrm{nat}} = \mathrm{v}_{\mathrm{div}}$). The second scenario expands on the first scenario through including the spatial variability of soil erodibility as function of land cover (i.e. $k_i = k_l$ with $l =$ 1, 2, 3). The third scenario additionally accounts for higher sediment supply in glaciated areas, thus assigning to the parameter α_g the value calibrated for the reference scenario. In the fourth scenario, hydropower reservoirs are additionally included by assuming that the coefficient β_i is equal to 1 for all cells *i* that are draining directly into reservoirs, and equal to zero elsewhere. Scenario five represents the configuration used for calibration (i.e. the “reference scenario”). Finally, in scenario six we impose the condition that sediment fluxes originated at cells flowing into water intakes have the same velocity of cells under natural flow conditions (i.e. $\mathrm{v}_{\mathrm{div}} = \mathrm{v}_{\mathrm{nat}}$).

Results

Sediment source fingerprinting

The log-ratio transformed biplots visualize the compositional difference between the samples derived from the three lithological units (Fig. 3). The full dataset on elemental compositions can be found in the supplementary material 1. The data shows that sediments from the calcschist/ meta-basalt unit are characterized by elements such as Fe_2O_3, TiO_2, MgO, MnO, Cr_2O_3, Sc and Ni, all of which can be expected to be enriched in sands sourced from marine sediments and basalts (e.g., Bhatia, 1983;

Rollinson, 2014). The elevated CaO contents can be linked to the carbonate component in the calcschists. Sediments derived from the gneisses and meta-sedimentary rocks are characterized by elements such as SiO_2, Na_2O, K_2O, Ba, Zr, Y and Nb. The glacial till sample taken from a moraine located within the meta-sedimentary catchments (Fig. 2) shows a mixed composition of the calcschist/ meta-basalt and meta-sedimentary origin (Fig. 3). This confirms that glacial tills are rather local deposits without significant contributions from higher (gneiss) lithologies. Accordingly, we infer that the glacial tills do not falsify the tributary sampling approach. High concentrations of Fe_2O_3, TiO_2, MgO, MnO, Cr_2O_3, Sc and Ni in the calcschist/ meta-basalt catchments are characteristic for this lithologic unit in both grain size fractions (Fig. 3a,b). In contrast, chemical characteristics may differ in the gneiss and meta-sedimentary catchments (Fig. 3). For example, the element Zr is distinctive for the gneisses in the <40 μm fraction, whereas it is characteristic for the meta-sedimentary rocks in the 40-400 μm fraction. This variability suggests that grain size may control certain elemental concentrations (e.g., von Eynatten et al., 2012). In the case of Zr and its most common mineral constituent zircon, this suggests that the gneisses contain more zircons in the finer grain size fraction, whereas in the meta-sedimentary rocks they are enriched in the coarser fraction.

The grain size distributions show similar patterns between samples from the same unit, but they differ substantially between the different source rock lithologies (Fig. 4). The three samples taken within the lowermost meta-sedimentary rocks (Torrent de Faran, La Manna and Gran Torrent) are the coarsest samples where on average ca. 90% of the grains are coarser than 400 μm (Fig. 4a). The samples taken within the middle reaches of the catchment (Gavil, Bornetta and Satarma; calcschists and meta-basalts) contain on average ca 70% of grains that are coarser than 400 μm. The samples from the Borgne de Ferpècle and Borgne d'Arolla, which drain the uppermost part of the catchment, underlain by gneisses, supply the finest grained material where on average only ca. 10% of the grains are coarser than 400 μm. The samples collected at the outlet of the Borgne catchment throughout the year show seasonally variable grain size distributions (Fig. 4b). The February sample contains exclusively sand-sized material of between 40 and 400 μm size. The fractions of grains coarser than 400 μm increase steadily in June (ca. 10%), July (ca. 40%) and August (ca. 90%). The October sample contains ca. 70% of grains coarser than 400 μm.

All elements in each grain size fraction underwent a statistical discrimination selection. In the 40-400 μm fraction, mass conservation is not fulfilled for P_2O_5, Zr and Y, whereas MgO, CaO, Na_2O, K_2O, TiO_2, P_2O_5, MnO, Ba, Zr, Y and Nb do not pass the Kruskal-Wallis-H-test to distinguish amongst the lithological units. Of the remaining elements SiO_2, Al_2O_3, Fe_2O_3, Cr_2O_3, Ni, Sr and Sc, stepwise DFA identified Ni, Al_2O_3, Sc, Sr and SiO_2 to provide greatest discrimination between the three sources. . In the <40 μm fraction, only Sr and Y do not fulfil the principle of mass conservation, but no element passes the Kruskal-Wallis-H-test. This poor statistical performance suggests that in this grain size fraction bulk geochemistry does not provide a suitable discrimination between the three sources. The compositional biplots suggest that this is mostly due to the chemical similarity of the gneiss and meta-sedimentary lithologies, whereas the calcschist/ meta-basalt signature is more distinct. Consequently, the selection of statistically robust elements as input parameters for the mixing model is not straightforward for the <40 μm fraction. Stepwise DFA was performed regardless of the Kruskal-Wallis-H-test results on all mass-conserving elements. DFA suggested a combination of Cr, Al_2O_3, Ba and Nb to provide maximal discrimination between the three sources.

According to this statistical selection, the elements Ni, Al_2O_3, Sc, Sr and SiO_2 in the 40-400 µm fraction and Cr, Al_2O_3, Ba and Nb for the <40 µm fraction are used as input parameters for the mixing model.

The results of the mixing modelling using the 40-400 µm fraction (Table 3) show a consistent dominance (71-84%) of material derived from the gneisses of the Dent Blanche unit located in the uppermost reaches of the catchment. Contributions of the meta-sedimentary rocks of the Middle Penninic Briançonnais (15-25%) and the calcschists/ meta-basalts of the Upper Penninic Piedmont-Liguria Ocean (1-4%) are less significant.

The mixing model yields seasonal compositional differences of the samples collected at the Borgne outlet in February, June, July, August and October (Fig. 5): between June and August, the relative contribution of the uppermost reaches (gneisses) decreases, while the relative contribution of the meta-sedimentary rocks increases.

The results of the mixing modelling using the <40 µm fraction (Table 4) also show a dominant contribution (78-87%) of material derived from the Dent Blanche gneisses. The contribution of meta-sedimentary rocks (15-25%) slightly increases in the summer months as well, whereas sediment from the calcschists/ meta-basalts is relatively low during the entire year (5-7%).

Although the statistical element selection is problematic for the <40 µm fraction and the source contribution uncertainties are generally higher than for the 40-400 µm fraction (Fig. 5), both mixing models yield identical results within uncertainty.

Modelling of sediment source dynamics

The parameters values resulting from the different model calibrations are quite similar indicating that the model performs relatively well against overfitting (see Table A2 in the supplementary material 2). In terms of model performances, Table A3 shows several goodness of fit measures of the leave-one-year-out calibration-validation approach. The daily Nash-Sutcliffe efficiency, for example, ranges from approximately 0.5 to 0.7 over the calibration periods although it is lower over the validation periods, ranging from 0.3 to 0.5. The monthly Nash-Sutcliffe efficiency is higher ranging from 0.5 to 0.9 over the validation period. These results show that the model is satisfactory in reproducing the observed dataset and that the model complexity is appropriate given the short observation dataset. Among the four cross-validation tests, the optimal parameter set used in the following analysis, chosen on the basis of minimum root mean squared error in validation, results from the test referred to as C1-V1 (Table A1, Table A3 in supplementary material 2).

Goodness of fit measures such as root mean squared error (RMSE), Nash-Sutcliffe efficiency (NS), mass balance relative error (MBRE), and correlation coefficient (ρ) are computed for calibration and validation based on observed and simulated daily and mean monthly SSL values (Table 2). The conceptual model reproduces fairly well SSL at the outlet of the Swiss Rhône catchment (Fig. 6, Table 2), especially at the monthly scale. In calibration, NS is equal to 0.54 and 0.80 at the daily and monthly scale respectively. In validation, the model maintains similarly good performances with NS equal to 0.51 at the daily scale and 0.79 at the monthly scale. Likewise, values of correlation coefficients above 0.7 and 0.9 respectively at the daily and monthly scale, indicate good correlation between simulated and observed SSL both in calibration and in validation (Table 2). While the model performs well during summer months, when SSL reaches its highest values, it overestimates SSL during low flow conditions (Fig. 6, right), as confirmed by the MBRE (Table 2).

In all three lithological units in the Borgne basin, snowmelt is the dominant hydrological process (Fig. 7). In the uppermost gneiss unit, ice melt contributes relatively more to runoff than erosive rainfall (Fig. 7c). Conversely, the contribution of erosive rainfall increases in the lowermost meta-sedimentary unit (Fig. 7a). This reflects the temperature gradients and spatial distribution of glaciers in the system. In the lower reaches of the catchment, warmer temperatures lead to higher amounts of precipitation in the form of rain compared to the higher, colder parts of the catchment. Model results indicate that in all three lithological units, the relative contribution of ice melt has increased since the mid 1980s (Fig. 7). The same pattern was observed on a larger scale in the entire Swiss Rhône catchment by Costa et al. (2018a), who explained this increase by accelerated glacial retreat following a significant temperature increase in the mid 1980s; as well as for the Borgne itself (Bakker et al., 2018).

In the first scenario, sediment supply is simulated as a function of hydroclimatic forcing only. The result suggests high contributions of all three units during the summer months (Fig. 8). In July, the months of the highest snow- and ice melt, the sediment load of the Borgne should be derived by up to 40% from gneisses and by 30% each from the meta-sedimentary and the calcschist/meta-basalt units. In winter, snow- and ice melt are negligible, and the upper part of the catchment is covered by snow, limiting the amount of erosive rainfall. In these months, the model simulates a dominant, but generally low sediment supply from the lowermost meta-sedimentary rocks only (Fig. 8), because in this modelling framework we do not account for sediment fluxes entrained by streamflow along channels (which may be dominant in the winter months due to high snow cover) or released from hydropower system operations. In the second scenario we include erodibility through land cover. Bare bedrock is more common in the uppermost part of the catchment, which is underlain by gneisses, whereas the lower meta-sedimentary and calcschists/ meta-basalt units are partially protected by vegetation cover. Consequently, the contribution of the gneiss unit increases significantly in this scenario (Fig. 9, Table 5). The contribution of the gneiss unit, where most of the glaciers in the catchment are located, increases in the third scenario (Fig. 9), because the large sediment supply typical of glaciated areas is accounted for. The rise in the relative contribution of the gneiss unit to sediment and water fluxes occurs mainly during the summer months (Fig. 9), when snow cover extent is low, and subglacial/proglacial sediment evacuation by ice-melt is at its highest. In the fourth scenario, which includes sediment trapping in Lac de Dix, the contribution of the calcschists and meta-basalts to the total sediment at the outlet of the Borgne decreases slightly to the benefit of gneisses (Fig. 9, Table 5).

In the fifth scenario, which represents the scenario closest to the actual conditions, the seasonal pattern of sediment contribution is substantially different to all the other scenarios (Fig. 9). In this scenario, the impact of water abstraction schemes is included by allowing the storage of sediment in the reservoirs and (temporarily) in the catchment, due to a reduced sediment transport capacity (i.e. $\beta_i = 0.5$ for all cells *i* located in areas draining to water intakes), and by allowing reduced sediment transfer rates to downstream reaches due to reduced transport capacity (i.e. $v_{nat} \neq v_{div}$). The optimization used in the calibration procedure finds a much smaller value for the velocity of the sediment fluxes originated in areas affected by water diversions than those originated in areas under natural flow regime: roughly 5 x 10^{-3} m s^{-1} (430 m day^{-1}) and 0.8 m s^{-1} (69 km day^{-1}) respectively. As a consequence, average travel times of sediment originated upstream of water intakes are equal to roughly three months (Fig. 10b). This is much longer than that of sediment generated in the unregulated fraction of the catchment, which model results indicate to be shorter than 1 day (Fig. 10a). As a result, sediment from the uppermost gneiss unit, which hosts most of the water abstraction schemes (Fig. 1), reaches the catchment outlet almost three months after being generated, resulting in a delayed signal with a higher relative contribution during winter (Fig. 9). In addition, due to within-river sediment storage, the contribution of the gneiss source rocks decreases at the annual scale (Table 5). In scenario six results in identical values for an annual relative contribution from the three lithological units (Table 5), but it yields a different seasonal distribution (Fig. 9). This is as expected, because the velocity of the sediment originated in the regulated areas in the catchment is forced to be equal to the transfer velocity of material generated in the unregulated areas.

None of the model scenarios accurately mirrors the source contributions inferred from fingerprinting (Fig. 11). Both mixing models (<40 and 40-400 µm) show a general dominance of sediment derived from gneiss sources in the system (~80% on average). Similarly, the model scenarios predict the highest contribution to be derived from gneiss sources (51% on average, whilst metasedimentary contribute ~23% and calcschists/ meta-basalts contribute ~26%). However, the model substantially underestimates the contribution of the gneiss unit (on average by roughly 30%) and overestimates the contribution of calcschists/ meta-basalts (on average by roughly 20%) and metasedimentary rocks (on average by roughly 8%).

Scenario five performs better than the other scenarios (Fig. 12). Mean monthly values of relative contribution, simulated at the sampling months in different scenarios are compared with observations by means of correlation coefficients and mean absolute errors (Fig. 12). Both metrics indicate that scenario five reproduces better than other scenarios the contribution of the three sediment sources. In particular, correlation coefficients suggest that scenario five better represents the temporal evolution of the relative contribution (Fig. 12). Results indicate that, by including the delayed contribution of sediment produced in areas regulated by water intakes, scenario five is the only scenario capable of mimicking the substantial contribution of sediment derived from the most upstream gneisses unit during winter months (Fig. 12).

Discussion

Possible grain size effects

The discrepancy between model simulations and observations of relative contributions of the three lithological units could arise from the different spatial availability of sand-sized sediment, which is the grain size targeted in this study. We showed a distinct seasonal grain size variation in the sampled sediment at the catchment outlet with coarser grains occurring in the summer months (Fig. 4b). This grain size variability at the outlet mirrors the annual water discharge pattern typically observed in such an Alpine catchment. With the onset of more rapid snow- and ice melt in summer, the water discharge peaks in the months between May and September, increasing the sediment transport capacity and facilitating the transport of larger grains (Tucker & Slingerland, 1991). However, such an effect is complicated here by the impacts of hydropower operations, as rates of flushing of water intakes are low in June, rise to a maximum in August and fall to November.

Whilst grain size distributions of sediment produced by glacial erosion can be highly variable, glacial outwash is generally known to contain large amounts of finely crushed sand and silt particles (Bagnold & Barndorff-Nielsen, 1980; Blott & Pye, 2001; Krumbein, 1934; Stephenson et al., 1988). Although the gneisses are the mechanically strongest lithology (Niggli & de Quervain, 1936) with theoretically very low erodibilities (Kühni & Pfiffner, 2001), significantly more fine-grained sediment might be produced in this part of the catchment due to intense glacial erosion. Indeed, the gneiss unit supplies more sand-sized sediment (40-400 μm) than the calcschist/ meta-basalt and the meta-sedimentary samples (Fig. 4a). In contrast, erosion in the lower reaches of the catchment is dominated by mass wasting and fluvial processes (Lambiel et al., 2016; Reynard et al., 2012), which tend to produce coarser-grained sediment. In particular the lowermost meta-sedimentary catchments supply high amounts of material coarser than 400 μm (Fig. 4a). Sediment supplied from the calcschist/ meta-basalt unit still contains some fine-grained sediment, which is probably due to the presence of more glaciers and lithologies with a higher erodibility compared to the meta-sedimentary unit (Kühni & Pfiffner, 2001). The grain size distributions of Borgne outlet samples throughout the year 2016 furthermore confirm a relationship between the grain size distribution and the composition at the outlet. With coarser grains in transport during summer more meta-sedimentary material is detected. Furthermore, the sub-catchment source samples were only taken on one occasion. We therefore cannot exclude the possibility that even at the sub-catchment scale the sediment shows chemical variations depending on the exported grain size. These grain size variations on different temporal and spatial scales, although challenging to quantify (e.g., Smith & Blake, 2014; Laceby et al., 2017), should be investigated in more detail. Accordingly, we conclude that most of the misfit between the observations and the modelling results could be caused by spatially variable production of sand-sized sediment in the system, which is not quantified in enough detail and not included into the model.

Possible temperature signals

Despite the described discrepancies between fingerprinting results and suspended sediment modelling, the modelling framework allows for the qualitative assessment of the effects of hydroclimatic processes, sediment storage, and alterations of sediment transfer rates due to water extraction in headwater channels on the observed sediment source contributions at the outlet. In particular, the results from the sediment fingerprinting and mixing modelling approach suggest that the Dent Blanche gneisses contribute the greatest proportion of sediment (mean ~80%) to the catchment outlet throughout the year. Such high contributions can be expected due to summer ice melt, which predominantly affects the heavily glaciated gneiss unit. The sediment production and transfer model supports this by simulating high sediment supply in response to ice melt during the summer months (Figs. 8, 10). High contribution of glaciogenic material is further supported by the cosmogenic nuclide inventory of the Borgne as investigated by Stutenbecker et al. (2018). ^{10}Be concentrations as low as $5.02 \pm 0.47 \times 10^3$ atoms/g quartz were measured in quartz from river bed sand of the Borgne river outlet, which yield an exceptionally high denudation rate of 2.74 ± 0.56 mm/y (Stutenbecker et al., 2018). A high contribution of glaciogenic material, which commonly exhibits very low ^{10}Be concentrations, could explain the overall low ^{10}Be concentrations measured at the catchment outlet and the consequently high denudation rates (Delunel et al., 2014; Godard et al., 2012).

Recently, Costa et al. (2018a) showed that the contribution of ice melt increased significantly in the Swiss Rhône catchment in response to a basin-wide temperature increase larger than 1 °C in the mid 1980s. This is consistent with the accelerated glacial retreat observed in many Alpine glaciers during that period (Fischer et al., 2014; 2015), including the glaciers located in the Borgne catchment (Gabbud et al., 2016; GLAMOS, 2017). The analysis of hydroclimatic variables in this study mirrors this relative increase of ice melt on a sub-catchment scale (Fig. 9). Lane et al. (2017) showed a rapid increase in sediment export following the onset of rapid recession of the Haut Glacier d'Arolla in the mid 1980s, a major contributor to the Borgne; and similar findings were made for a set of further intakes downstream (Bakker et al., 2018) as well as in sedimentation in the Swiss Rhône delta of Lake Geneva (Lane et al., 2019). Bakker et al. (2018) found that despite significant flow abstraction, the majority of sediment, ranging from boulders to silt, delivered to intakes is transported downstream and sediment connectivity is maintained over the time-scale of decades.

Lane et al. (2019) confirmed that this signal could be seen in an elevated flux to and deposition in the Rhône delta from the 1980s. This interplay shows that with increasing temperatures and accelerating glacial retreat, higher contributions of glacial ice melt may lead to increased proportions of glaciogenic material entering the sediment routing system, and despite large-scale water management impacts, here related to hydropower. This is reflected in high contributions of gneisses at the Borne basin outlet.

Flow abstraction practices delays the arrival of climate signals downstream

Whilst hydroclimatic forcing provides a feasible explanation for the dominance of sediment derived from gneiss source rocks during the summer months, the equally high contribution of this unit observed during the winter months (Figs. 5, 10) is not yet fully accounted for. The model predicts little to no sediment supply during the winter months from this unit, because the hillslopes of the catchment are frozen and snow-covered, especially at higher altitudes. Indeed, during the sampling campaign in February 2016 snow cover extended across almost the entire catchment (SLF, 2016), eliminating possible contributions from erosive rainfall or snow-melt relating to the other units, found at lower altitudes. An explanation for the nonetheless high supply sediment from the gneiss unit during winter arises from model scenario five (Fig. 11). Although water abstraction and sediment trapping in the higher reaches of the catchment do not completely prevent the transfer of sand-sized particles to the outlet, the water management does cause a substantial delay in transfer of ca. four months (Figs. 9 and 12). Field observations suggest that intake flushing upstream, mainly within the gneisses, tends to leave drapes of fine sediment downstream, which is temporally stored within the main stream after abrupt flushing-event cessation and re-entrained with the onset of a following flushing event (Bakker et al., 2019). Consequently, our results suggest that the high contribution of sediment derived from the gneiss unit during winter is not caused by actual sediment supply from the (snow-covered or frozen) hillslopes, but due to the delayed transfer of sediment that is temporarily stored within the system. In Fig. 11, the shape of the curve of scenario five is the only one similar to the curves from fingerprinting results, suggesting that this model scenario, although not accurate, predicts the best overall patterns of sediment delivery.

Possible effects related to hydropower storage of sediment

None of the scenarios succeeds in explaining the overall very low contribution of calcschists and meta-basalts. The maximum contribution of these lithologies according to the mixing modelling is 6.8 ± 3.9 % (in July) and thus up to four times lower than the contribution predicted by the different scenarios. Because the calcschist/meta-basalt fingerprint is excellent and well distinguishable from the other two units (Fig. 3), it is unlikely that our approach failed to detect this sediment at the catchment outlet. Part of the explanation for the lack of the sediment may be provided by modelling scenario four. The reservoir lake Lac de Dix was built into the calcschist/ meta-basalt bedrock in Val d'Hérémence (Fig. 2). Sediment produced on the hillslopes of the 45 km^2 large, partially glaciated reservoir catchment gets directly trapped in the lake. In the modelling scenario four sediment is permanently trapped in the lake (over the investigated timescale). Results show that the reservoir trap reduces the contribution of calcschists/ meta-basalts from on average 30% in scenarios one to three to 20%. However, the relative contribution of the calcschist/ meta-basalt unit in scenario four is still one and a half (<40 µm) to three times (40-400 µm) larger than observations, suggesting that other factors which are not explicitly accounted in the model are responsible for the very limited contribution coming from this unit.

Limitations of both approaches

Although we showed that the combination of conceptual modelling and a field-based fingerprinting/mixing modelling approach offers the opportunity to compare and verify results and to qualitatively test the influence of different variables on the sediment dynamics, both methods used in this study have limitations.

Results from the fingerprinting/mixing modelling approach showed that grain size variations cannot be neglected both at the sub-catchment and the catchment scale. The wide grain size window adopted here (40-400 µm) should be divided into several, narrower grain sizes in order to better detect grain size changes throughout the year. Furthermore, we only sampled sediment from the sub-catchments on one occasion assuming that they would have a rather stable sedimentary fingerprint due to less intense anthropogenic impact and less sediment reworking. This simplification could contribute to the error in source endmember composition and therefore influence the mixing modelling results.

The conceptual model on sediment production and transfer has a fairly simple conceptual structure and some of the modelling assumptions could be improved if more information was available. In particular, the hypothesis that the hydropower reservoirs completely block the sediment could be softened by having more information about the management strategies. Moreover, although sediment transport velocities are expected to vary in space and time together with discharge (along streams) and/or overland flow (along hillslopes), the model includes solely the delayed transfer of sediment trapped in water intakes. In the current version of the model, we define the fraction of the sediment actually contributing to the suspended sediment load at the outlet (coefficient β_i) a-priori. We distinguish areas impounded by reservoirs

(β_i = 1) from areas impounded by water diversions (β_i = 0.5) and unregulated areas (β_i = 0). These values allow only for a coarse characterization of the sediment dis-connectivity in the catchment and channel system. In the presence of a bigger dataset these parameters could be calibrated. In particular, a value of the parameter greater than zero ($\beta_i > 0$) for the unregulated areas could represent the process of sediment storage within the catchment. Furthermore, sediment connectivity indexes, such the ones proposed by Cavalli et al. (2013) and Borselli et al. (2008) could be considered when increasing the spatial resolution of the model so to better represents topographic features such as contributing area, slope, flow path and topographic roughness, which are smoothed out at the current 500 m by 500 m resolution. The scarce data availability, restricted to only four years of daily data, might limit the ability of the model to properly reproduce the sediment formation and transfer in very diverse hydro-meteorological conditions with respect to the ones observed in the training datasets. Finally, the simplicity of the conceptual modelling framework as well as the limited data availability does not allow the simulation of the grain size effect, which appears to play a significant role in the sediment composition at the outlet of the catchment.

Conclusions

By combining a sediment fingerprinting approach with a conceptual, spatially distributed sediment production and transfer model, we are able to qualitatively infer the relative seasonal contributions of the different factors controlling sediment dynamics in the Alpine Borgne catchment. The study shows that the Borgne sediment is predominantly, ~80%, derived from the uppermost one third of the catchment, where sediment supply is controlled by glacial ice melt. This case study suggests that with increasing temperatures in response to climate change, rapidly retreating glaciers and potentially increased connectivity, glacial outwash is expected to remain the most important sediment source in the Borgne catchment. As glacier retreat is a widespread phenomenon in the Alps (e.g. Fischer et al., 2015), these considerations may apply to other catchments undergoing these changes, at least whilst glacier cover if sufficient to provide the meltwater needed to maintain sediment export (Lane et al., 2017).

Although the upper reaches of the Borgne catchment are impacted by flow abstraction, sediment is still being transferred through the system to reach the outlet of the catchment on annual basis. However, sediment transfer is delayed due to decreased sediment transport capacities, which could explain why glacial sediment is also dominating the system during the winter months. The Lac de Dix reservoir in Val d'Hérémence traps sediment produced in the middle reaches of the catchment, underlain by calcschists and meta-basalts, thereby explaining a lower contribution of this unit to the overall sediment budget. However, the actual observations cannot be adequately reproduced by the model simulations, which we interpret to be linked to spatially variable production of sand-sized sediment.

In addition, the work implies that the increase in sediment delivery from deglaciating catchments may well be countered by water management, but the extent to which this is the case depends on the nature of the water management scheme. Here, the hydropower system involved both a large dam and also a large number of water abstraction systems. Despite lowering transfer rates, the latter maintain sediment connectivity and this means that despite the catchment having very significant hydropower exploitation, the signal of climate change impacts on glaciogenic sediment production could still be identified at the catchment outlet (Lane et al., 2019).

We show that both the modelling and the fingerprinting approaches have limitations and could be improved by considering additional factors such as grain size distributions. However, only the combination of both methods offers the opportunity to verify the results from numerical modelling and to qualitatively assess the impacts of different drivers influencing the sediment yield at the catchment scale.

Acknowledgements

This study was funded by the Sinergia grant 147689 awarded to F. Schlunegger, S. Girardclos, S.N. Lane, J.-L. Loizeau and P. Molnar by the Swiss National Science Foundation. We thank Stéphanie Girardclos, Jean-Luc Loizeau and Tiago Adrião Silva for discussions and two anonymous reviewers for their constructive criticism and comments.

The authors declare that they have no conflict of interest.

References

Aitchison, J. (1983). Principal component analysis of compositional data. *Biometrika, 70*, 57-65. doi:10.1093/biomet/70.1.57

Aitchison, J. & Greenacre, M. (2002). Biplots of compositional data. *Applied Statistics, 51*, 375-392. doi:10.1111/1467-9876.00275

Anghileri, D., Botter, M., Castelletti, A., Weigt, H., & Burlando, P. (2018a). A comparative assessment of the impact of climate change and energy policies on Alpine hydropower. *Water Resources Research, 54,* 9144-9161. doi: 10.1029/2017WR022289

Anghileri, D., Castelletti, A., & P. Burlando, P. (2018b). Alpine hydropower in the decline of the nuclear era: exploring trade-offs between revenue and production in the Swiss Alps. *Journal of Water Resources Planning and Management* , *144-8*, 04018037. doi: 10.1061/(ASCE)WR.1943-5452.0000944

Anselmetti, F. S., Bühler, R., Finger, D., Girardclos, S., Lancini, A., Rellstab, C. & Sturm, M. (2007). Effects of Alpine hydropower dams on particle transport and lacustrine sedimentation. *Aquatic Sciences, 69*, 179-198. doi:10.1007/s00027-007-0875-4

Bagnold, R. A. & Barndorff-Nielsen, O. (1980). The pattern of natural size distributions. Sedimentology, 27, 199-207. doi:10.1111/j.1365-3091.1980.tb01170.x

Bakker, M. (2018). Morphodynamics and sediment transfer in a human-impacted alpine river. (Doctoral thesis, Université de Lausanne, Switzerland).

Bakker, M., Antoniazza, G., Odermatt, E. & Lane, S.N. (2019). Morpholoigcal response of an Alpine braided reach to sediment-laden flow events. *Journal of Geophysical Research Earth Surface*, 124, 1310-1328. doi: 10.1029/2018JF004811

Bakker, M., Costa, A., Silva, T. A., Stutenbecker, L., Girardclos, S., Loizeau, J.-L., […] & Lane, S. N. (2018). Combined flow abstraction and climate change impacts on an aggrading Alpine river. *Water Resources Research*, *54*, 223-242. doi:10.1002/2017WR021775

Bhatia, M. R. (1983). Plate tectonics and geochemical composition of sandstones. *The Journal of Geology, 91,* 611-627.

Blott, S. J. & Pye, K. (2001). Gradistat : a grain size distribution and statistics package for the analysis of unconsolidated sediments*. Earth Surface Processes and Landforms*, *26*, 1237-1248. doi:10.1002/esp.261

Borselli, L, Cassi, P & Torri, D (2008). Prolegomena to sediment and flow connectivity in the landscape: a GIS and field numerical assessment. *Catena, 75,* 268-277. doi: 10.1016/j.catena.2008.07.006

Cavalli, M., Trevisani, S., Comiti, F. & Marchi, L. (2013). Geomorphometric assessment of spatial sediment connectivity in small Alpine catchments. *Geomorphology, 188,* 31–41. doi:10.1016/j.geomorph.2012.05.007

Collins, A. L. & Walling, D.E. (2002). Selecting fingerprinting properties for discriminating potential suspended sediment sources in river basins*. Journal of Hydrology, 261*, 218-244. doi:10.1016/S0022-1694(02)00011-2

Collins, A. L., Walling, D. E. & Leeks, G. J. L. (1996). Composite fingerprinting of the spatial source of fluvial suspended sediment : a case study of the Exe and Severn river basins, United Kingdom. *Géomorphologie : relief, processus, environnement, 2,* 41-53. doi:10.3406/morfo.1996.877

Comas, M. & Thió-Henestrosa, S. (2011). CoDaPack 2.0: a stand-alone multi-platform compositional software. In J. J. Egozcue, R. Tolosana-Delgado, M. I. Ortego (Eds.), *CoDaWork'11: 4th International Workshop on Compositional Data Analysis*. Saint Feliu de Guixols, Girona, Spain.

Comiti, F. (2012). How natural are Alpine mountain rivers? Evidence from the Italian Alps. *Earth Surface Processes and Landforms, 37*, 693-707. doi:10.1002/esp.2267

Costa, A., Molnar, P., Stutenbecker, L., Bakker, M., Silva, T. A., Schlunegger, F., … Girardclos, S. (2018a). Temperature signal in suspended sediment export from an Alpine catchment. *Hydrology and Earth System Sciences, 22*, 509-528. doi:10.5194/hess-22-509-2018.

Costa, A., Anghileri, D. & Molnar, P. (2018b). Hydroclimatic control on suspended sediment dynamics of a regulated Alpine catchment: a conceptual approach, *Hydrology and Earth System Sciences, 22*, 3421-3434. doi:10.5194/hess-22-3421-2018.

Delunel, R., van der Beek, P. A., Bourlès, D. L., Carcaillet, J. & Schlunegger, F. (2014). Transient sediment supply in a high-altitude Alpine environment evidenced through a 10Be budget of the Etages catchment (French Western Alps). *Earth Surface Processes and Landforms, 39*, 890-899. doi:10.1002/esp.3494

Denaro, S., Anghileri, D., Giuliani, M., & Castelletti, A. (2017). Informing the operations of water reservoirs over multiple temporal scales by direct use of hydro-meteorological data. *Advances in Water Resources, 103*, 51-63. doi: 10.1016/j.advwatres.2017.02.012

Fatichi, S., Rimkus, S., Burlando, P., Bordoy, R. & Molnar, P. (2015). High-resolution distributed analysis of climate and anthropogenic changes on the hydrology of an Alpine catchment. *Journal of Hydrology, 525,* 362-382. doi:10.1016/j.jhydrol.2015.03.036

Federal Office of Topography Swisstopo (2011). Geologische/tektonische/hydrogeologische Karte der Schweiz 1:500000. Wabern, Switzerland.

Fischer, M., Huss, M., Barboux, C. & Hoelzle, M. (2014). The new Swiss Glacier Inventory SGI2010: relevance of using high-resolution source data in areas dominated by very small glaciers. *Arctic, Antarctic, and Alpine Research, 46*, 933-945. doi:10.1657/1938-4246-46.4.933

Fischer, M., Huss, M. & Hoelzle, M. (2015). Surface elevation and mass changes of all Swiss glaciers 1980-2010. *Cryosphere, 9,* 525-540. doi:10.5194/tc-9-525-2015

Francipane, A., Ivanov, V. Y., Noto, L. V., Istanbulluoglu, E., Arnone, E. & Bras, R.L. (2012). tRIBS-Erosion: A parsimonious physically-based model for studying catchment hydro-geomorphic response. *Catena, 92*, 216–231. doi:10.1016/j.catena.2011.10.005

Frei, C. (2014). Interpolation of temperature in a mountainous region using nonlinear profiles and non–Euclidean distances, *International Journal of Climatology, 34*, 1585-1605. doi:10.1002/joc.3786

Frei, C., Schöll, R., Fukutome, S., Schmidli, J. & Vidale, P. L. (2006). Future change of precipitation extremes in Europe: An intercomparison of scenarios from regional climate models. *Journal of Geophysical Research, 111,* D06105. doi:10.1029/2005JD005965

Gabbud, C. & Lane, S. N. (2016). Ecosystem impacts of Alpine water intakes for hydropower: the challenge of sediment management. *WIREs Water, 3*, 41-61. doi:10.1002/wat2.1124

Gabbud, C., Micheletti, N. & Lane, S. N. (2016). Response of a temperate Alpine valley glacier to climate change at the decadal scale. *Geografiska Annaler A: Physical Geography, 98*, 81-95. doi:10.1111/geoa.12124

Galelli, S. & Castelletti, A. (2013). Tree-based iterative input variable selection for hydrological modeling. *Water Resources Research, 49*, 4295-4310.

doi:10.1002/wrcr.20339

Garzanti, E., Resentini, A., Vezzoli, G., Andò, S., Malusà, M. G. & Padoan, M. (2012). Forward compositional modelling of Alpine orogenic sediments. *Sedimentary Geology, 280,* 149-164. doi:10.1016/j.sedgeo.2012.03.012

Girardclos, S., Fiore, J., Rachoud-Schneider, A.-M., Baster, I. & Wildi, W. (2005). Petit-Lac (western Lake Geneva) environment and climate history from deglaciation to the present: a synthesis. *Boreas, 34*, 417-433. doi:10.1080/03009480500231385

GLAMOS (2017). *Gletscherberichte (1881-2017): Die Gletscher der Schweizer Alpen*. Jahrbücher der Expertenkommission für Kryosphärenmessnetze der Akademie der Naturwissenschaften Schweiz (SCNAT), Zürich, retrieved at https://www.glamos.ch/publikationen#tab-uebersicht/E23%2F16

Hallet, B., Hunter, L. & Bogen, J. (1996). Rates of erosion and sediment evacuation by glaciers: A review of field data and their implications. *Global and Planetary Change*, *12,* 213-235. doi: 10.1016/0921-8181(95)00021-6

Hock, R. (2003). Temperature index melt modelling in mountain areas. *Journal of Hydrology, 282*, 104-115. doi:10.1016/S0022-1694(03)00257-9

Hovius, N., Stark, C. P. & Allen, P. A. (1997). Sediment flux from a mountain belt derived by landslide mapping. *Geology, 25*, 231-234. doi:10.1130/0091-7613(1997)025<0231:SFFAMB>2.3.CO;2

Korup, O. (2009). Linking landslides, hillslope erosion, and landscape evolution. *Earth Surface Processes and Landforms, 34*, 1315-1317. doi:10.1002/esp

Krumbein, W. C. (1934). Size frequency distributions of sediments. *Journal of Sedimentary Petrology,4,* 65-77. doi:10.1306/D4268EB9-2B26-11D7-8648000102C1865D

Laceby, J. P., Evrard, O., Smith, H. G., Blake, W. H., Olley, J. M., Minella, J. P. G. & Owens, P. N. (2017). The challenges and opportunities of addressing particle size effects in sediment source fingerprinting: A review. *Earth-Science Reviews, 169*, 85-103.

Laceby, J. P. & Olley, J. (2015). An examination of geochemical modelling approaches to tracing sediment sources incorporating distribution mixing and elemental correlations. *Hydrological Processes, 29,* 1669-1685. doi:10.1002/hyp.10287

Lambiel, C., Maillard, B., Kummert ,M., & Reynard, E. (2016). Geomorphology of the Hérens valley (Swiss Alps). *Journal of Maps, 12,* 160-172. doi:10.1080/17445647.2014.999135

Lane, S. N., Bakker, M., Balin, D., Lovis, B. & Regamey, B. (2014). Climate and human forcing of Alpine river flow. In A. J. Schleiss, G. De Cesare, M. J. Franca, M. Pfister (Eds.), *Proceedings of the International Conference on Fluvial Hydraulics (RiverFlow 2014)* (pp. 7-15). London: CRC Press Taylor & Francis Group.

Lane, S.N., Bakker, M., Costa, A., Girardclos, S. Loizeau, J-L., Molnar, P., Silva, T., Stutenbecker, and Schlunegger, F. (2019). Making stratigraphy in the Anthropocene: climate change impacts and economic conditions controlling the supply of sediment to Lake Geneva. Forthcoming in *Scientific Reports.*

Lane, S. N., Bakker, M., Gabbud, C., Micheletti, N. & Saugy, J.-N. (2017). Sediment export, transient landscape response and catchment-scale connectivity following rapid climate warming and Alpine glacier recession. *Geomorphology, 277,* 210-227. doi:10.1016/j.geomorph.2016.02.015

Loizeau, J.-L. & Dominik, J. (2000). Evolution of the upper Rhone river discharge and suspended sediment load during the last 80 years. *Aquatic Sciences, 62*, 54-67. doi:10.1007/s000270050075

MeteoSwiss (2013). *Documentation of MeteoSwiss grid–data products daily precipitation (final analysis): RhiresD*. Retrieved from http://www.meteoswiss.admin.ch/content/dam/meteoswiss/de/service-und-publikationen/produkt/raeumliche-daten-niederschlag/doc/ProdDoc_RhiresD.pdf

Micheletti, N., Lambiel, C. & Lane, S. N. (2015). Investigating decadal-scale geomorphic dynamics in an alpine mountain setting. *Journal of Geophysical Research: Earth Surface, 120,* 2155-2175. doi:10.1002/2015JF003656

Micheletti, N. & Lane, S. N. (2016). Water yield and sediment export in small, partially glaciated Alpine watersheds in a warming climate. *Water Resources Research, 52,* 4924-4943. doi:10.1002/2016WR018774

Montgomery, D. R., Brandon, M. T. (2002). Topographic controls on erosion rates in tectonically active mountain ranges. *Earth and Planetary Science Letters, 201,* 481-489. doi:10.1016/S0012-821X(02)00725-2

Morgan, R. P. C. & Duzant, J.H. (2008). Modified MMF (Morgan–Morgan–Finney) model for evaluating effects of crops and vegetation cover on soil erosion. *Earth Surface Processes and Landforms, 32,* 90-106. doi: 10.1002/esp.1530

Niedrist, G., Tasser, E., Lüth, C., Dalla Via, J. & Tappeiner, U. (2009). Plant diversity declines with recent land use changes in European Alps. *Plant Ecology, 202*, 195-210. doi:10.1007/s11258-008-9487-x

Orand, A. (1986). Etude des affluents du Leman et de son emissaire. In C.I.P.E.L., Commission Internationale Pour La Protection Des Eaux Du Leman Contre La Pollution (Ed.), *Rapports Sur Les Études et Recherches Entreprises Dans Le Bassin Lémanique* (pp. 91-104), Lausanne.

Reynard, E., Lambiel, C. & Lane, S. N. (2012). Climate change and integrated analysis of mountain geomorphological systems. *Geographica Helvetica, 67*, 5-14. doi:10.5194/gh-67-5-2012

Rollinson, H. R. (2014). Using geochemical data: Evaluation, presentation, interpretation. London, New York: Routledge, Taylor & Francis Group.

Scherrer, S. C. & Appenzeller, C. (2006). Swiss alpine snow pack variability: Major patterns and links to local climate and large-scale flow. *Climate Research, 32,* 187-

199. doi:10.3354/cr032187

Schmid, S. M., Fügenschuh, B., Kissling, E. & Schuster, R. (2004). Tectonic map and overall architecture of the Alpine orogen. *Eclogae Geologicae Helvetiae, 97*, 93-117. doi:10.1007/s00015-004-1113-x

Schwarb, M. (2000). *The Alpine precipitation climate evaluation of a high-resolution analysis scheme using comprehensive rain-gauge data* (Doctoral thesis, ETH Zürich, Switzerland).

Serquet, G., Marty, C., Dulex, J.-P. & Rebetez, M. (2011). Seasonal trends and temperature dependence of the snowfall/precipitation-day ratio in Switzerland. *Geophysical Research Letters, 38*, L07703. doi:10.1029/2011GL046976

Sherriff, S. C., Franks, S.W., Rowan, J.S., Fenton, O. & Ó'hUallacháin, D. (2015). Uncertainty-based assessment of tracer selection, tracer non-conservativeness and multiple solutions in sediment fingerprinting using synthetic and field data. *Journal of Soils and Sediments, 15,* 2101-2116. doi:10.1007/s11368-015-1123-5

SLF (2016). *Weekly report on snow condititions (5.-11. of February 2016) by the WSL Institute for Snow and Avalanche Research SLF*. Retrieved from https://www.slf.ch/fileadmin/user_upload/import/weeklyreports_old/pdfs/2015-16/wochenbericht_2016-02-05_FR.pdf (in French).

Smith, H. G. & Blake, W. H. (2014). Sediment fingerprinting in agricultural catchments: A critical re-examination of source discrimination and data corrections.

Geomorphology, 204, 177-191. doi:10.1016/j.geomorph.2013.08.003

Stallard, R. F. (1998). Terrestrial sedimentation and the carbon cycle: Coupling weathering and erosion to carbon burial*. Global Biogeochemical Cycles, 12*, 231-257. doi:10.1029/98GB00741

Steinmeier, C. (2013). *CORINE Land Cover 2000/2006 Switzerland. Final Report*. Swiss Federal Institute for Forest, Snow and Landscape Research WSL, Birmensdorf, Switzerland.

Stephenson, D. A., Flemming, A. H. & Mickelson, D. M. (1988). Glacial deposits. In W. Back, J. S. Rosenheim & P. R. Seaber (Eds.), *Hydrogeology: The Geology of North America* (pp. 301-314). Boulder, Colorado, USA: Geological Society of America.

Stutenbecker, L., Delunel, R., Schlunegger, F., Silva, T. A., Šegvić, B., Girardclos, S., … Christl, M. (2018). Reduced sediment supply in a fast eroding landscape? A multi-proxy sediment budget of the upper Rhône basin, Central Alps. *Sedimentary Geology, 375*, 105-119. doi:10.1016/j.sedgeo.2017.12.013.

Tucker, G. E. & Slingerland, R. (1996). Predicting sediment flux from fold and thrust belts. Basin Research 8 : 329-349. doi:10.1046/j.1365-2117.1996.00238.x

von Blanckenburg, F. (2005). The control mechanisms of erosion and weathering at basin scale from cosmogenic nuclides in river sediment. *Earth and Planetary Science Letters, 237,* 462-479. doi:10.1016/j.epsl.2005.06.030

von Eynatten, H., Tolosana-Delgado, R. & Karius, V. (2012). Sediment generation in modern glacial settings: Grain-size and source-rock control on sediment composition. *Sedimentary Geology, 280,* 80-92. doi:10.1016/j.sedgeo.2012.03.008

Weber, C., Peter, A. & Zanini, F. (2007). Spatio-temporal analysis of fish and their habitat: A case study on a highly degraded Swiss river system prior to extensive rehabilitation. *Aquatic Sciences, 69,*162-172. doi:10.1007/s00027-007-0912-3

Willett, S. D. (1999). Orogeny and orography: The effects of erosion on the structure of mountain belts. *Journal of Geophysical Research, 104,* 28957-28981. doi:10.1029/1999JB900248

Wischmeier, W.H. & Smith, D. D (1978). Predicting rainfall erosion losses – a guide to conservation planning. Agricultural Handbook, 537, Washington D.C., 58 p.

Wohl, E. (2006). Human impacts to mountain streams. *Geomorphology, 79,* 217-248. doi:10.1016/j.geomorph.2006.06.020

Tables

Table 1: Summary of investigated properties (geology, glaciers and land cover) of the three lithological units.

Lithological unit	Surface area (km^2)	Glaciated area (km^2)	Land cover (%)				
			Open	Forests	Shrubs	Pastures	Other
Gneisses	118 (31%)	38.0 (32%)	91.8	1.2	7.0	0	0
Calcschists/meta-basalts	124 (32%)	1.4 (1%)	55.2	9.9	26.9	4.7	3.3
Meta-sedimentary rocks	143 (37%)	2.5 (2%)	24.6	34.4	31.6	8.3	1.1
All	385	41.9 (11%)	55.2	16.6	22.2	4.6	1.4

Table 2: Goodness of fit measures for the conceptual model of suspended sediment load in calibration (C1: May 2013 – April 2016) and in validation (V1: May 2016 – April 2017), at the daily and the monthly time scale: root mean squared error (RMSE), Nash-Sutcliffe efficiency (NS), mean balance relative error (MBRE), and correlation coefficient (ρ).

	Calibration – C1 01 May 2013 – 30 April 2016	Validation – V1 01 May 2016 – 30 April 2017
daily		
RMSE [ton day^{-1}]	12562.37	7367.06
NS [0 - 1]	0.54	0.51
MBRE [%]	-19.10%	-41.56%
ρ [-1 +1]	0.74	0.73
monthly		
RMSE [ton day^{-1}]	3770.70	2336.79
NS [0 - 1]	0.80	0.79
MBRE [%]	-19.12%	-41.37%
ρ [-1 +1]	0.91	0.96

Table 3: Results from mixing modelling using the 40-400 μm grain size fraction and stepwise DFA-selected input parameters (Ni, Al_2O_3, Sc, Sr, SiO_2). Values represent the mean value and the standard deviation (uncertainty) of 10000 iterations.

Borgne sample	Contribution of gneisses (%)	Contribution of calcschists/ meta-basalts (%)	Contribution of meta-sedimentary rocks (%)	Goodness of fit (GOF)
February	84.4 ± 3.3	0.8 ± 0.4	14.8 ± 3.1	67%
June	84.1 ± 3.2	0.9 ± 0.5	14.9 ± 3	69%
July	72.1 ± 3.8	3.6 ± 1.2	24.3 ± 3.2	74%
August	71.2 ± 6.5	3.8 ± 2.1	25.1 ± 4.8	75%
October	84.4 ± 3.3	1.1 ± 0.6	14.5 ± 3	75%

Table 4: Results from mixing modelling using the <40 μm grain size fraction and stepwise DFA-selected input parameters (Cr2O3, Al2O3, Ba, Nb). Values represent the mean value and the standard deviation (uncertainty) of 10000 iterations.

Borgne sample	Contribution of gneisses (%)	Contribution of calcschists/ meta-basalts (%)	Contribution of meta-sedimentary rocks (%)	Goodness of fit (GOF)
February	86.8 ± 6.5	4.6 ± 2.8	8.6 ± 6.1	67%
June	83.2 ± 8.2	5.3 ± 3.1	11.5 ± 8	70%
July	80.2 ± 8.7	6.8 ± 3.9	13 ± 8.6	69%
August	78.6 ± 9.7	6.5 ± 3.7	14.9 ± 9.9	68%
October	80 ± 8.8	6.7 ± 3.8	13.3 ± 8.8	68%

Table 5: Mean annual relative contribution and difference to the “reference scenario” of the three main lithological units to the sediment at the outlet of the Borgne for the scenarios from one to six.

Scenario		Mean annual relative contribution and difference to "reference scenario" (%)					
		Meta-sedimentary rocks		Calcschists / meta-basalts		Gneisses	
1	Spatial variability in **hydroclimatic forcing**	35	11	31	8	34	-19
2	Spatial variability in hydroclimatic forcing and **erodibility**	19	-5	30	7	51	-2
3	Spatial variability in hydroclimatic forcing and erodibility + **higher sediment supply in glaciated areas**	18	-6	29	6	53	0
4	Spatial variability in hydroclimatic forcing and erodibility + higher sediment supply in glaciated areas + **reservoirs**	18	-6	20	-3	62	9
5	Spatial variability in hydroclimatic forcing and erodibility + higher sediment supply in glaciated areas + reservoirs + **water diversions**	24	-	23	-	53	-
6	Spatial variability in hydroclimatic forcing and erodibility + higher sediment supply in glaciated areas + reservoirs + water diversions - **sediment flux velocity constant in space**	24	0	23	0	53	0

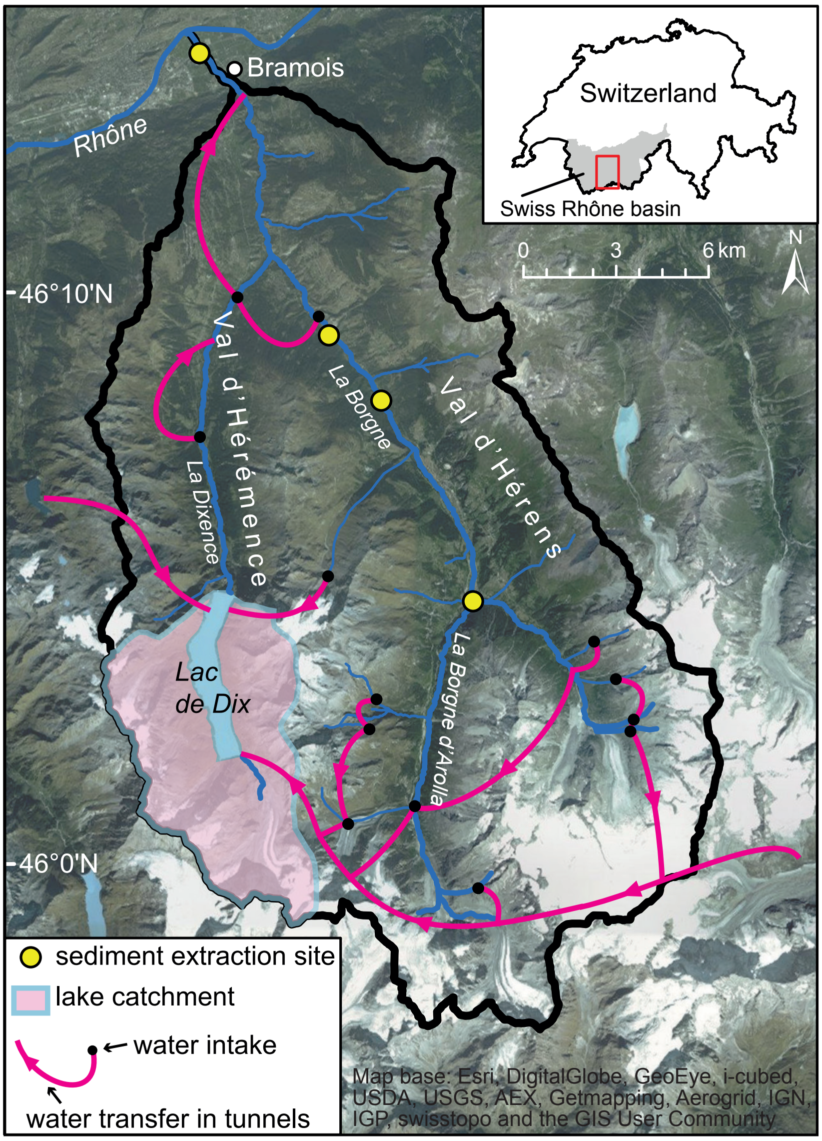

Fig. 1: Map of the Borgne tributary basin and its fluvial network (in blue). Water abstraction tunnels that transfer water within the river or into the reservoir lake Lac de Dix are indicated after Margot et al. (1992). Topographic base map created with ArcGIS® software. Copyright © Esri

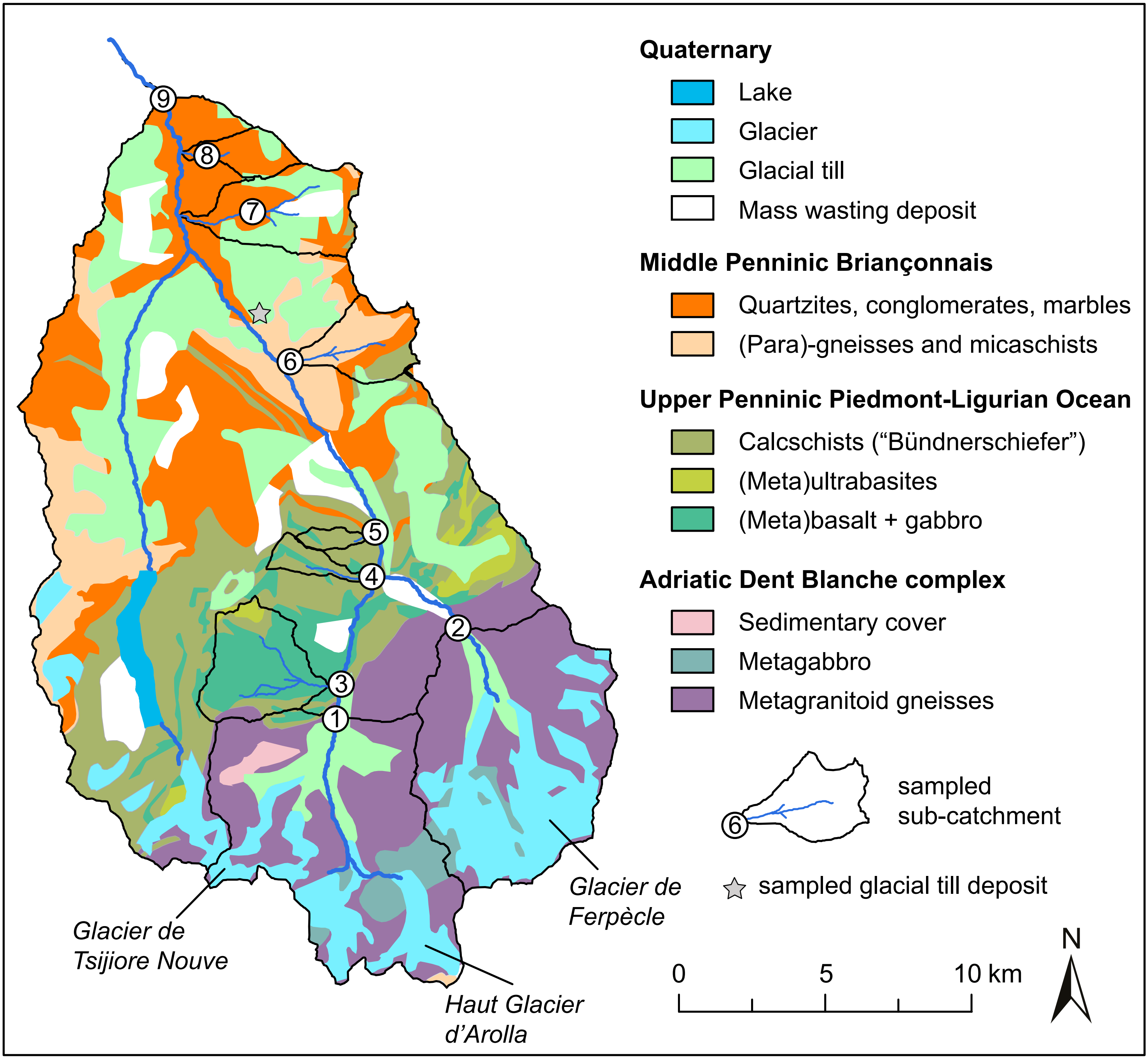

Fig. 2: Geological map of the Borgne basin showing the tripartition of the catchment into meta-sedimentary rocks of the Middle Penninic Briançonnais unit (lowermost reaches), calcschists and meta-basalts of the Upper Penninic Piedmont-Liguria Ocean (middle reaches) and gneisses of the Adriatic Dent Blanche complex (uppermost reaches). The fluvial network, the sampled sub-catchments and sample locations are shown as well. The numbers of the samples refer to the following streams:
Sample 1 = Borgne d’Arolla, sample 2 = Borgne de Ferpècle, sample 3= Satarma, sample 4 = Bornetta, sample 5 = Gavil, sample 6 = Grand Torrent, sample 7 = La Manna, sample 8 = Torrent de Faran, sample 9 = Borgne outlet close to the village of Bramois. The sample indicated with a star was taken within a glacial till deposit (see text for further explanation).

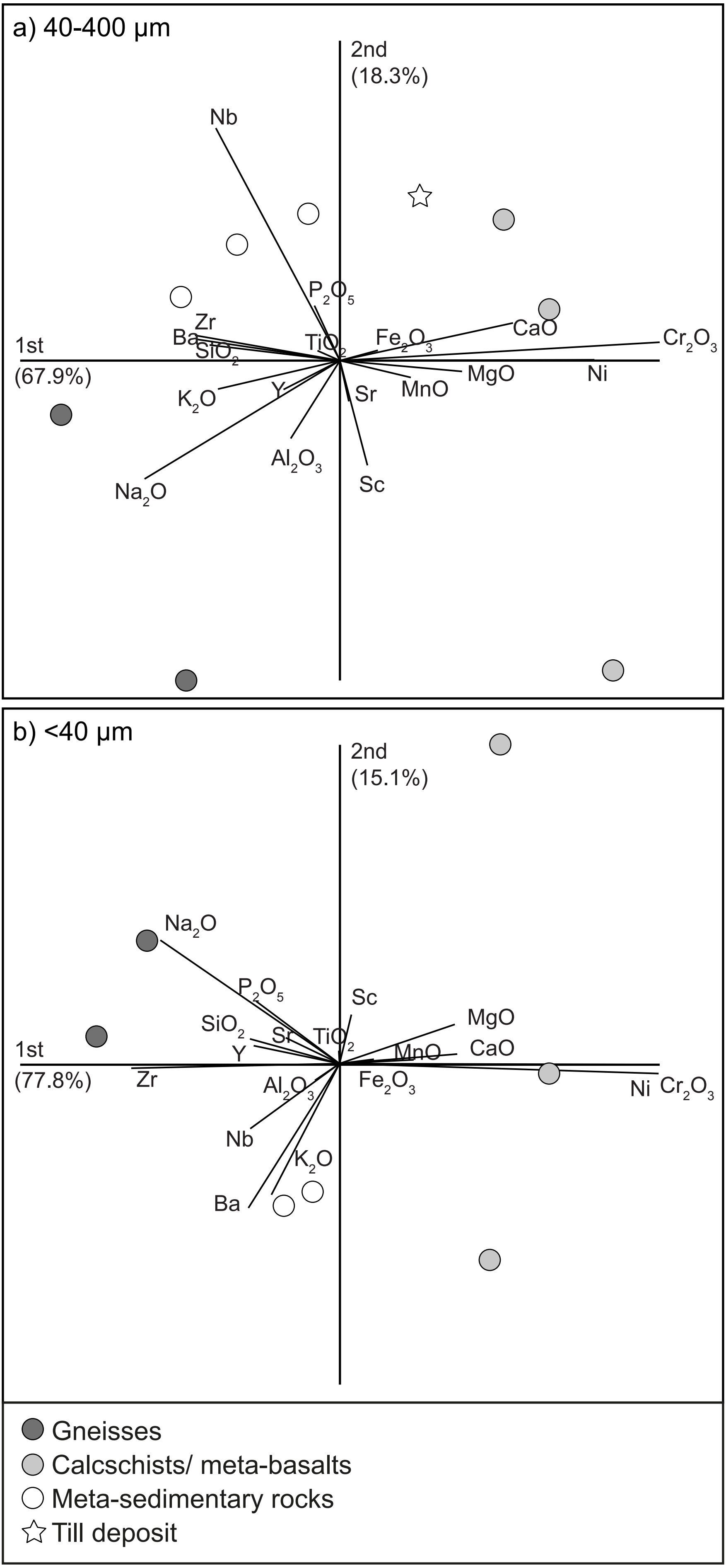

Fig. 3: Log-ratio transformed compositional biplots derived from principal component analysis for the grain size fraction of 40-400 µm (a, upper panel) and<40 µm (b, lower panel).

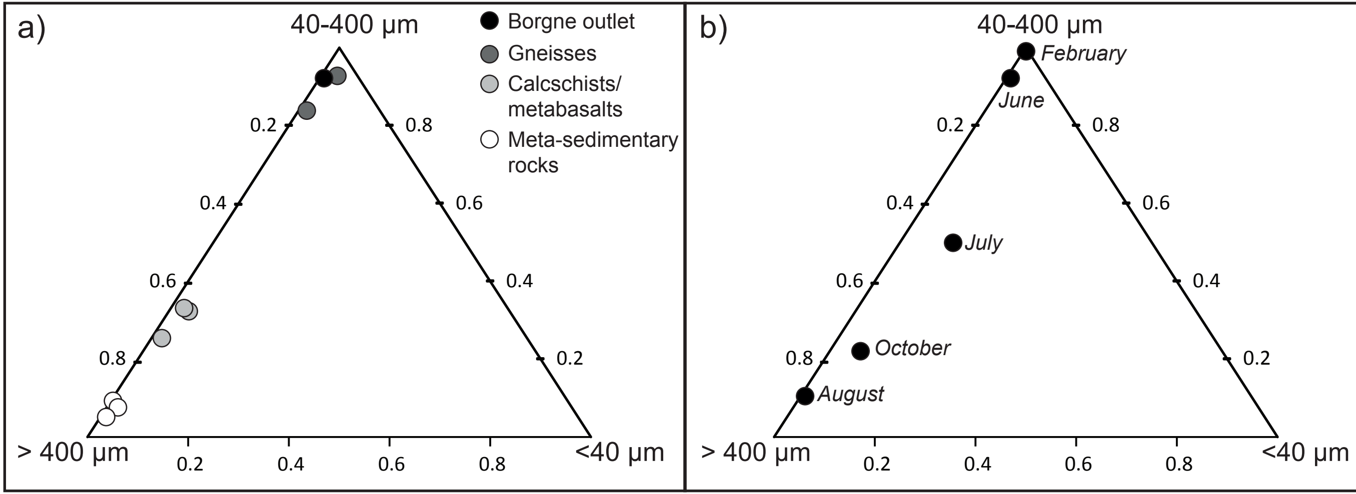

Fig. 4: Ternary plot displaying grain size distributions obtained through wet sieving. a) Grain size distribution of all tributary basin samples, taken on 1st of June 2016, and the corresponding sample taken on the same day at the Borgne outlet. The tributary samples form three distinctive clusters depending on the lithological unit they were taken from. Note that the June outlet sample grain size distribution resembles the cluster of sediment taken from the gneiss unit. b) Variation of grain size distributions from samples taken at the Borgne outlet during the months of February, June, July, August and October, 2016. Note the general increase of coarse sediment (>400 µm) during the year.

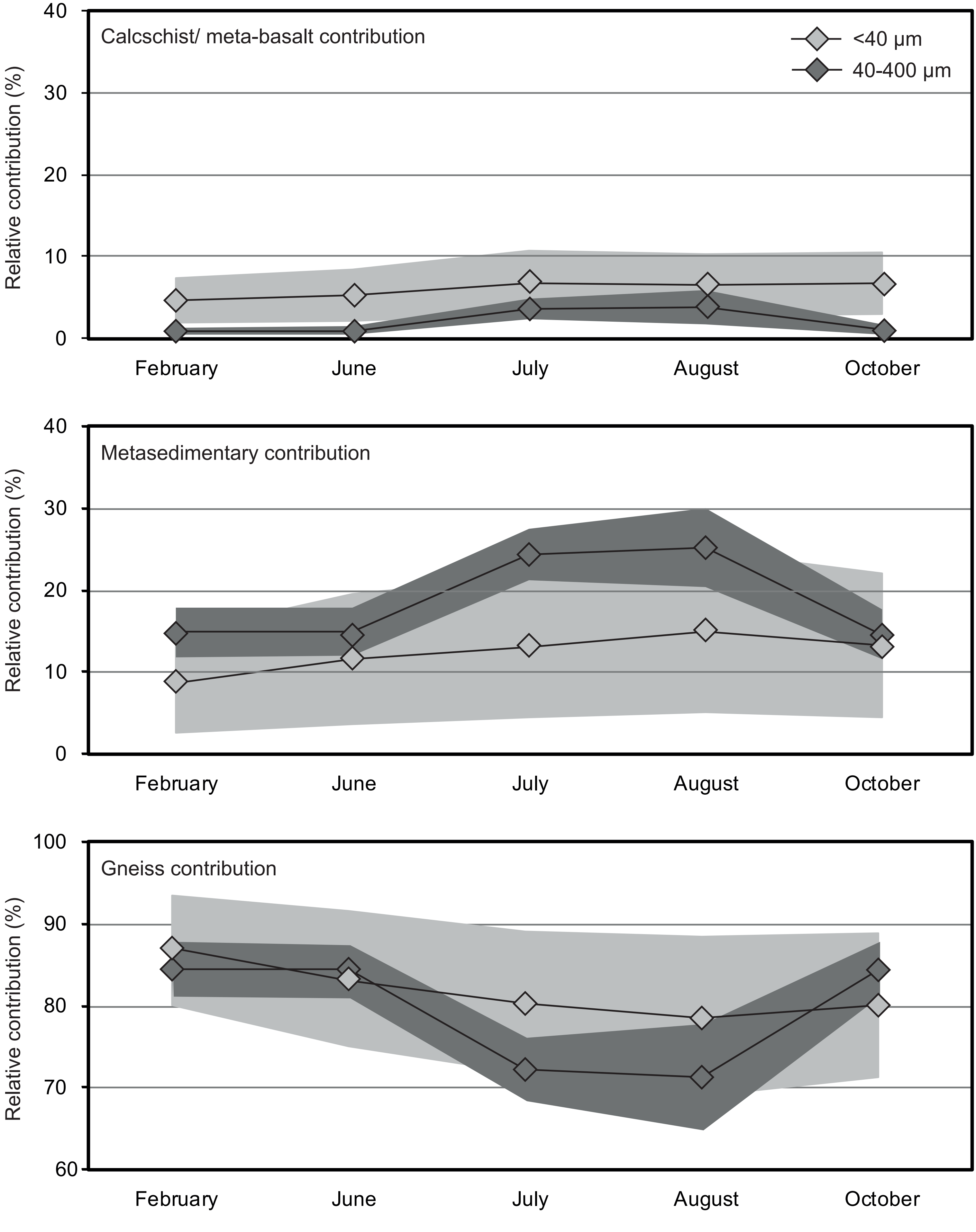

Fig. 5: Visualization of the relative contributions of calcschist/meta-basalts, metasedimentary rocks and gneisses to the sediment of different grain size collected at the basin outlet in different months of 2016.

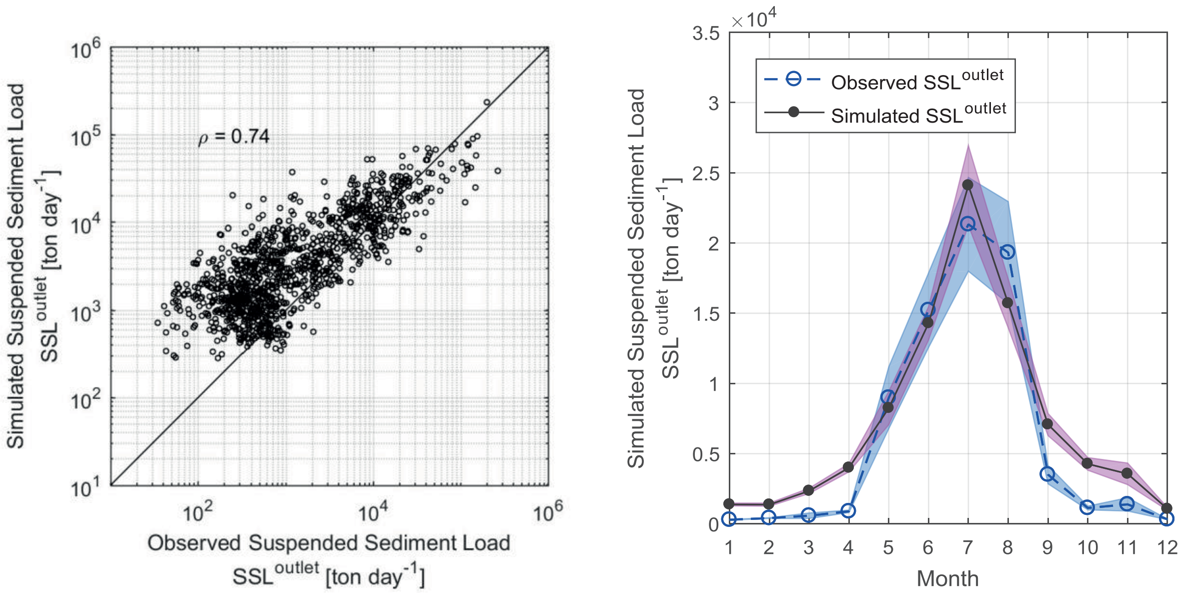

Fig. 6: Observed and simulated suspended sediment load at the outlet of the Swiss Rhône catchment for the calibration period May 2013 – April 2016 (left). Scatter plot of observed and simulated daily values (right). Mean monthly observed values with blue dashed line with circles and simulated values with black line with dots; shaded areas r epresent ± standard errors.

Fig. 6: Observed and simulated suspended sediment load at the outlet of the Swiss Rhône catchment for the calibration period May 2013 – April 2016 (left). Scatter plot of observed and simulated daily values (right). Mean monthly observed values with blue dashed line with circles and simulated values with black line with dots; shaded areas r epresent ± standard errors.

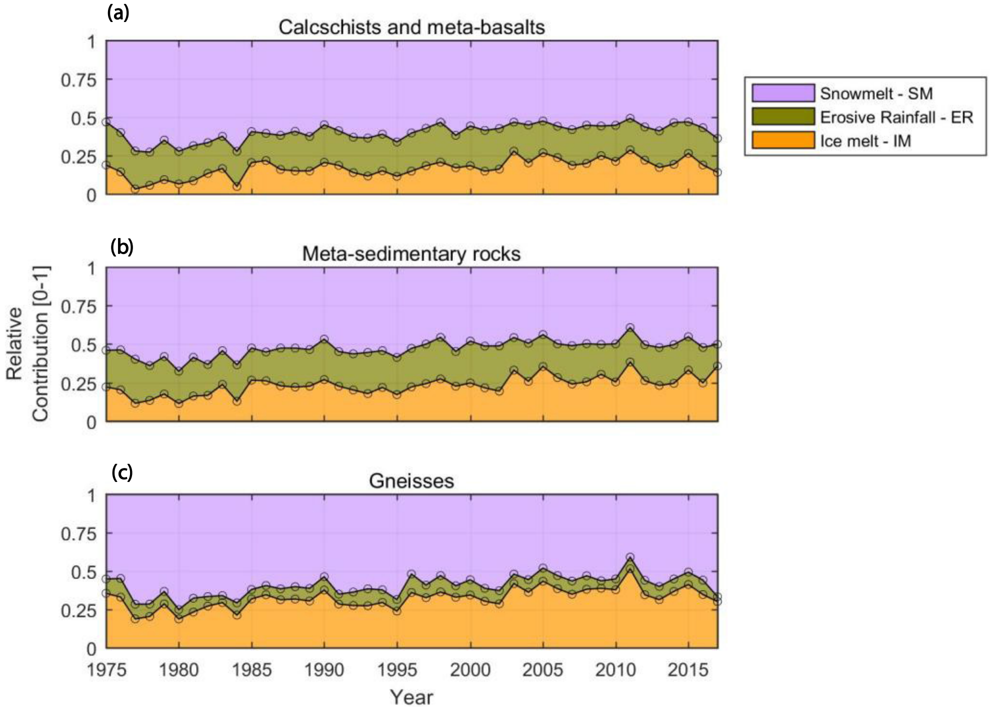

Fig. 7: Time series (1975-2017) of the relative contribution of total annual erosive rainfall ER, snowmelt SM and ice melt IM within each lithological unit (a, b and c).

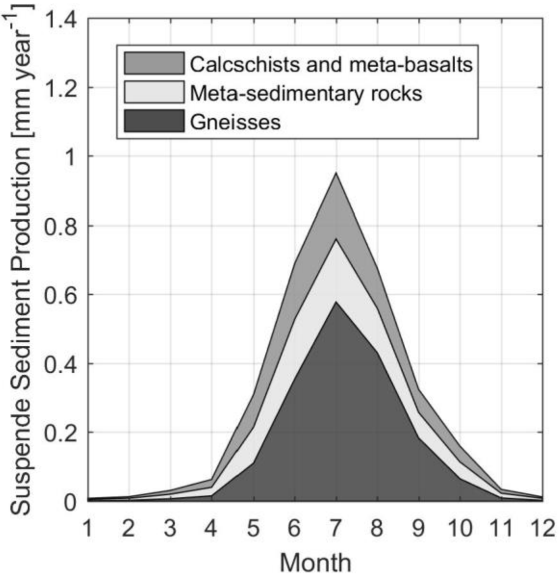

Fig. 8: Mean monthly suspended sediment generated at each lithological unit of the Borgne catchment for the period 1975-2017, considering only spatial variability of hydroclimatic forcing (scenario one): erosive rainfall, snowmelt and ice melt.

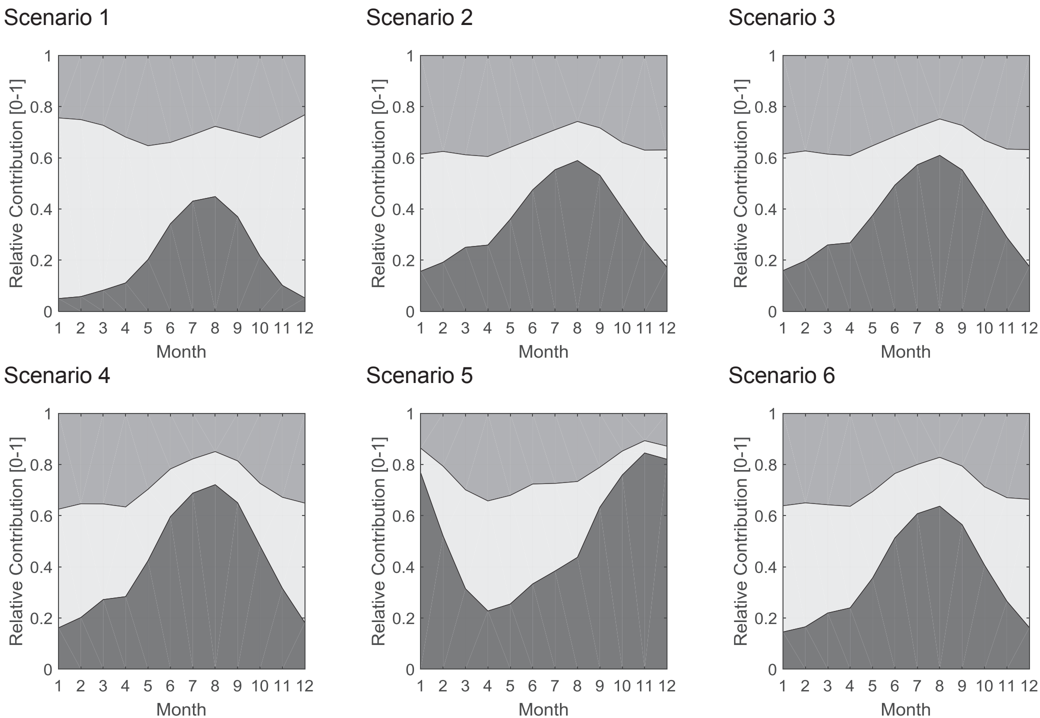

Fig. 9: Mean monthly relative contribution of the three lithological units to the suspended sediment yield at the outlet of the Borgne basin for the six different scenarios (scenario one to six) for the period 1975-2017.

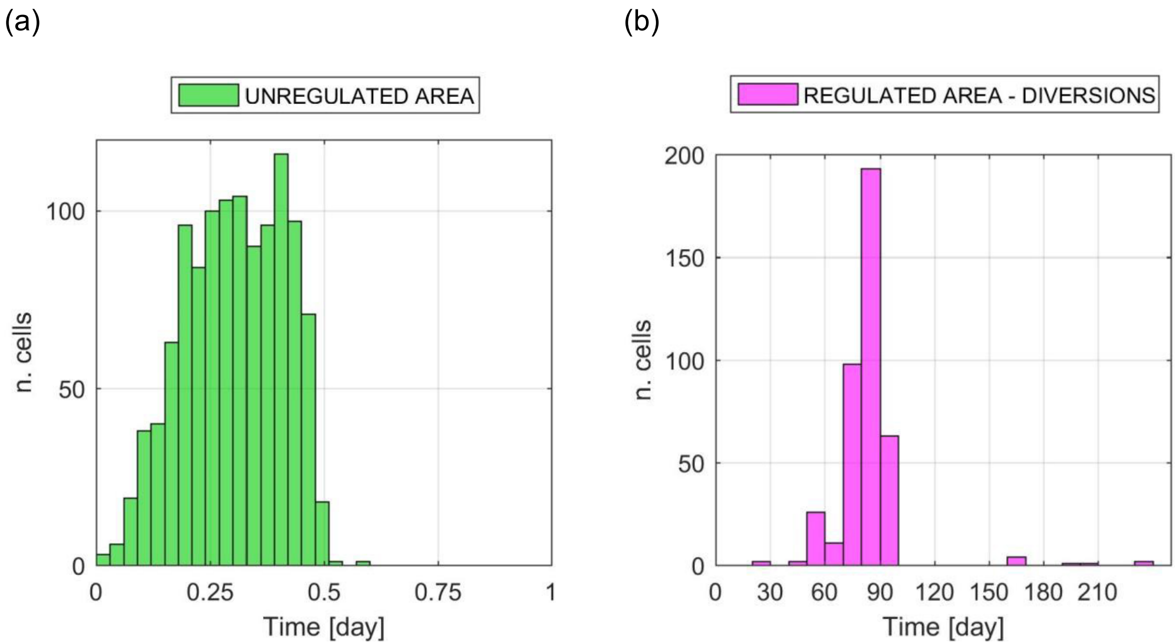

Fig. 10: Frequency distribution of the travel time of sediment fluxes originated from (a) unregulated areas and (b) regulated areas upstream from flow abstraction.

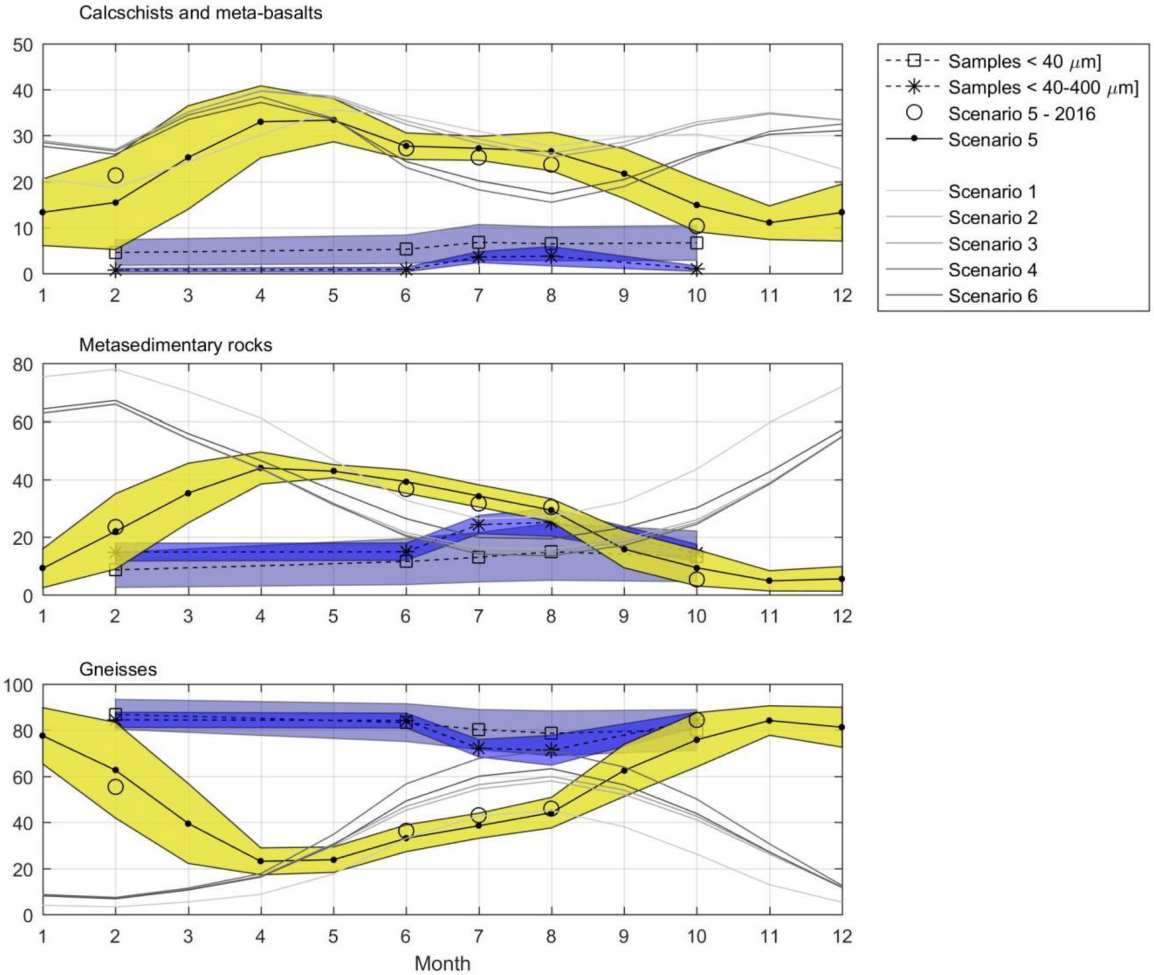

Fig. 11: Comparison of relative source contributions derived from the mixing modelling and the six scenarios of the conceptual model. Dark and light blue shaded areas represent errors of the mixing modelling. Scenario five is depicted with a black line with dots, while scenarios one to four and six are shown with grey lines. Yellow shaded area represent ± standard error of the model simulation in scenario five.Black circles represent mean monthly values of relative contribution simulated in scenario five, corresponding to samples of 2016.

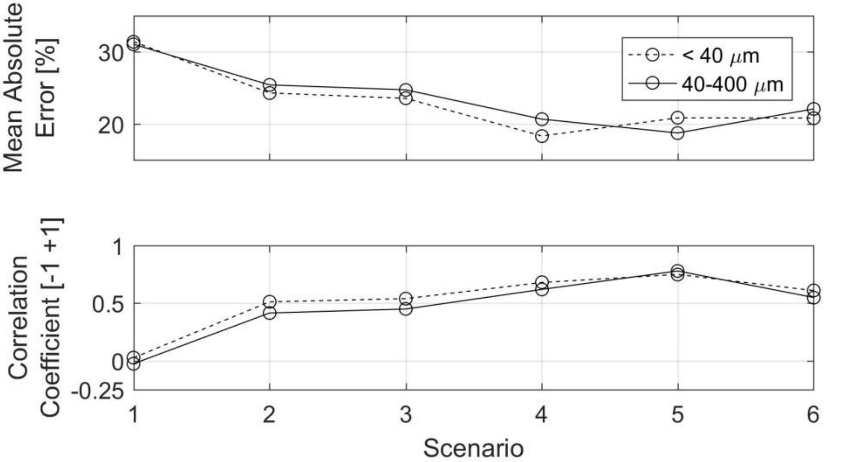

Fig. 12: Goodness of fit measures for the conceptual model in reproducing the relative contributions of the three lithological units for the six different scenario.